ELSEVIER

Journal of Organometallic Chemistry 490 (1995) 51–70

Journal of Organometallic Chemistry

Bis(di-t-butylphosphino)methane complexes of rhodium: homogeneous alkyne hydrosilylation by catalyst-dependent alkyne insertion into Rh–Si or Rh–H bonds. Molecular structures of the dimer $[(dtbpm)RhCl]_2$ and of the silyl complex $(dtbpm)Rh[Si(OEt)_3](PMe_3)$ ☆

Peter Hofmann [a,*], Claudia Meier [a], Wolfgang Hiller [a], Maximilian Heckel [a], Jürgen Riede [a], Martin U. Schmidt [b]

[a] *Anorganisch-chemisches Institut der Technischen Universität München, Lichtenbergstrasse 4, D-85747 Garching, Germany*

[b] *Institut für Anorganische Chemie der Rheinisch-Westfälischen Technischen Hochschule Aachen, Professor-Pirlet-Strasse 1, D-52056 Aachen, Germany*

Received 4 July 1994

Abstract

The homogeneous, Rh-catalysed hydrosilylation of but-2-yne with triethoxysilane has been studied. All rhodium complexes employed as catalyst precursors contain $^tBu_2PCH_2P^tBu_2$ ("dtbpm") as a chelating ligand. The crystal and molecular structure of the dimer $[(dtbpm)RhCl]_2$ (**10**) has been determined by X-ray diffraction. Complex **10** is shown to be a sluggish catalyst in hydrosilylation reactions of hex-1-ene, whereas but-2-yne is hydrosilylated more rapidly. A much more efficient and highly selective catalyst is **10** with added PPh_3, equivalent to the use of monomeric $(dtbpm)RhCl(PPh_3)$. (*E*)-2-Triethoxysilylbut-2-ene is formed exclusively and with high turnover numbers in this case. For both **10** and its PPh_3 derivative, the 14-electron fragment [(dtbpm)RhCl], formed by dissociation processes, is the most likely active intermediate in a Harrod–Chalk-type catalytic cycle. The PPh_3 dissociation equilibrium has been studied in detail for $(dtbpm)RhCl(PPh_3)$ and its thermodynamic parameters have been determined. With rhodium alkyl complexes as catalyst precursors, a different type of alkyne hydrosilylation catalysis, involving direct alkyne insertion into the Rh–Si bond of an intermediate rhodium silyl complex, $(dtbpm)Rh[Si(OEt)_3](PMe_3)$ (**14**), has been found. Complex **14** was synthesized independently from $(dtbpm)RhMe(PMe_3)$ and characterized by X-ray diffraction. It is an equally active catalyst itself, yielding (*E*)-2-triethoxysilylbut-2-ene as the major product (90%) from but-2-yne and $HSi(OEt)_3$ (turnover number 1000 per 30 min). The insertion step of the alkyne into the Rh–Si bond of **14** and the formation of two stereoisomeric rhodium vinyl complexes were established independently for $MeO_2CC{\equiv}CCO_2Me$ as a more reactive alkyne substrate. A catalytic cycle is proposed for this unprecedented hydrosilylation reaction. The synthesis of the η^3-benzyl complex $(dtbpm)Rh(\eta^3\text{-}CH_2C_6H_5)$ (**23**) is described. This compound allows an alternative, more efficient access to the new silyl complex $(dtbpm)Rh[Si(OEt)_3](PMe_3)$.

Keywords: Rhodium; Alkyne hydrosilylation; Catalysis; X-ray structure; Benzyl; Allyl

1. Introduction

Hydrosilylation reactions of alkenes, alkynes or related heteroatom-containing, unsaturated functional groups represent an industrially important class of catalytic processes performed on a large scale [1]. Although recent work [2] clearly indicates heterogeneous Pt metal catalysis for typical industrial platinum mediated hydrosilylations, the generally accepted mechanism for homogeneous hydrosilylation catalysis by transition metal complexes [3] implies some variant of the so called Harrod–Chalk scenario [4]. There, insertion of the unsaturated substrate (e.g. the alkene or alkyne) into a metal–hydride bond of an intermediate *cis*-hydridosilyl complex is assumed, leading to *cis*-alkylsilyl or *cis*-alkenylsilyl transients, which subsequently undergo reductive elimination of the silylated product.

☆ Dedicated to Professor Hans Hofmann on the occasion of his 65th birthday.

* Corresponding author.

SSDI 0022-328X(94)05173-9

The necessary metal hydride species are preformed by oxidative addition of a silane Si–H bond to an electronically and coordinatively unsaturated metal fragment ML_n (i.e. by Si–H bond activation).

There are two important categories of such highly reactive transition metal intermediates ML_n, which are particularly prone to bond activation chemistry and catalysis: dicoordinate d^{10} ML_2 and tricoordinate d^8 ML_3 complexes. Both possess only 14 valence electrons, their ground-state geometries being linear and T-shaped, respectively [5]. In contrast to, e.g., d^8 ML_4 fragments, oxidative addition (e.g. bond activation) reactions or two-electron–ligand association processes to d^{10} ML_2 and d^8 ML_3 species lead to electronically and coordinatively still unsaturated products (16 valence electrons), which can easily undergo subsequent intra- or intermolecular transformations, making d^{10} ML_2 and d^8 ML_3 fragments especially suitable for catalytic reaction cycles.

By introducing the tailor-made chelating bisphosphines bis(di-*t*-butylphosphino)methane ($^tBu_2PCH_2P^tBu_2$, dtbpm [6]) and its cyclohexyl analog ($Cy_2PCH_2PCy_2$, dcpm [7]), into the chemistry of 14-electron d^{10} ML_2 complexes (M = Ni^0, Pd^0, Pt^0, L_2 = chelating bisphosphine), we have recently been able to generate highly strained four-membered ring fragments **1** in situ and to study their chemistry. With dtbpm and (mutatis mutandis) dcpm, these "hot" and short-lived intermediates have sufficient lifetimes to display various unprecedented intermolecular bond activation reactions towards C–H, Si–H, C–Si, C–F and C–C bonds [8,9]. Moreover, unusual ligand coordination modes [10,11], various metal-centred coupling processes involving small organic molecules [12] and interesting catalytic properties have been found in these systems. The chemistry of reactive intermediates **1** is predominantely caused by their (ligand-enforced) abnormally small P–M–P bite angle of around 75° (deviating around 105° from the normal 180° L–M–L angle of d^{10} ML_2 systems) and by their concomitant anomalous valence orbital structure, which we have detailed elsewhere [13].

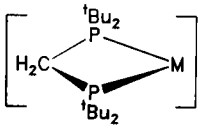

M = Ni, Pd, Pt

1

Within the d^8 ML_3 group of complexes, short-lived 14-electron intermediates of the general type $[(PR_3)_2MX]$ (M = Rh, Ir; X = anionic ligand) are well established as the relevant transients in many metal-induced, catalytic or stoichiometric transformations of organic substrates [14]. Suffice it to mention here the well documented role of the prototype $[(PPh_3)_2RhCl]$ fragment, formed by PPh_3 dissociation from Wilkinson's complex $(PPh_3)_3RhCl$ in the catalytic cycle of homogeneous hydrogenation reactions [15], or the role of photogenerated intermediates $[(PMe_3)_2RhCl]$ and their congeners in C–H activation chemistry [16]. It is not surprising, of course, that such molecules or their relatives also have been found to catalyse hydrosilylation [17].

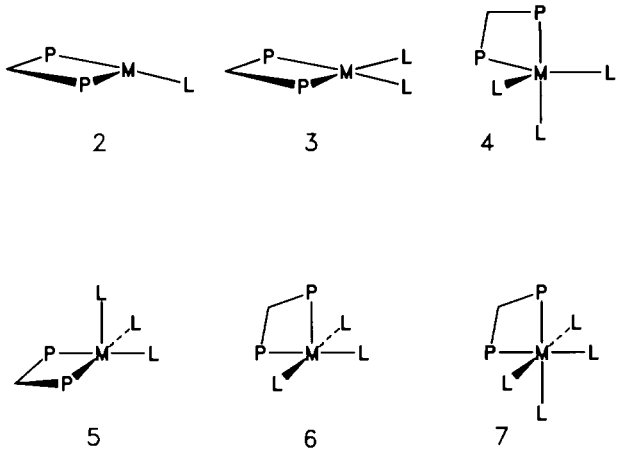

M = d^8 or d^6 metal center

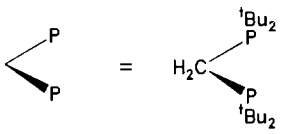

Obviously and in contrast to d^{10} systems **1**, two *cis*-ligands in a T-shaped d^8 ML_3 unit **2** can adopt the small bite angles of diphosphinomethane ligands without suffering from extreme distortions. The same is true for their potential four-, five- and six-coordinate reaction products and derivatives **3**, **4**, **5**, **6** and **7** with square-planar, trigonal bipyramidal, square pyramidal or octahedral environments and oxidation states I or III.

As there is theoretical [18] and experimental [19] evidence that mixed d^8 ML_2L' complexes such as $[(PR_3)_2MX]$ might prefer T-shape geometries with a less symmetrical C_s *cis* structure rather than the C_{2v}-type *trans* arrangement for two monodentate phosphine ligands, it seemed of interest to study d^8 ML_3 intermediates or derivatives thereof, in which bis(di-*t*-butylphosphino)methane functions as a *cis*-chelating ligand. Therefore, we set out to synthesize various dtbpm complexes of rhodium and iridium in order to investigate the consequences of (i) *cis*-chelation, (ii) a small bite angle of ca. 75°, (iii) steric bulk at the P centres and (iv) strong phosphorus donor character, on the metal reactivity of either tricoordinate 14-electron

intermediates **8** or of square-planar 16-electron complexes **9** (M = Rh^I, Ir^I; X = anionic ligand, L = neutral ligand).

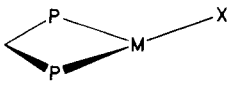

8

M = Rh, Ir

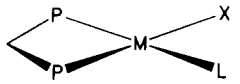

9

Some time ago we reported [20] the synthesis of the chloro-bridged rhodium dimer $[(dtbpm)RhCl]_2$ (**10**), which, according to molecular weight determinations in solution, undergoes facile dissociation into monomeric (probably solvent-stabilized) 14-electron fragments [(dtbpm)RhCl] (**8**; M = Rh, X = Cl). Compound **10** has served as a convenient starting material for the synthesis of a variety of square-planar dtbpm complexes of the general formula (dtbpm)RhCl(L) (L = neutral donor ligand), and as a typical example we have described the molecular structure of its PMe_3 derivative **11**, $(dtbpm)RhCl(PMe_3)$ [20].

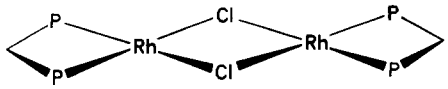

10

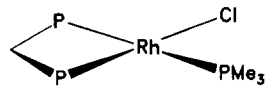

11

The main objective of the work presented here is to describe two mechanistically different types of alkyne hydrosilylation reactions catalysed by **10** and by derivatives of this compound. Hydrosilylation by **10** proceeds via the monomeric 14-electron fragment [(dtbpm)RhCl], generated either by dissociation of the chloro-bridged dimer or from suitable precursor complexes **9** by dissociation of L, and is in accord with the normal Harrod–Chalk picture. In the course of these investigations, however, we also prepared catalyst precursor complexes, which lead to efficient homogeneous alkyne hydrosilylation reactions via direct insertion of alkynes into the Rh–Si bond of an intermediate Rh–silyl complex.

In this paper we describe these different systems and their reactive behaviour, together with relevant molecular structure determinations, including the synthesis, isolation and X-ray structure of the novel Rh–silyl complex $(dtbpm)Rh[Si(OEt)_3](PMe_3)$, which inserts alkynes into its Rh–Si bond.

2. Results

The starting material for all compounds was the chloro-bridged dimer $[(dtbpm)RhCl]_2$ (**10**). In solution, this compound undergoes complete dissociation into (certainly solvent coordinated [21]) monomeric fragments [(dtbpm)RhCl], as evidenced by our earlier molecular weight determinations [20]. Facile dissociation of **10**, in accord with related systems carrying comparably bulky chelating diphosphinoalkane ligands [22], was anticipated not only on the basis of steric crowding around the metal centres in the dimer, but also from MO model calculations [20], which had predicted a weakening of Rh–μ–Cl bonds for P–Rh–P angles smaller than 90°, as they are enforced by diphosphinomethane ligands. Because we considered structural details of the dimer **10** in its solid-state structure to be relevant for its behaviour in solution, we determined the crystal and molecular structure of this compound.

Crystals of **10**, suitable for an X-ray structure determination, could be grown by slowly cooling a saturated solution of **10** in acetone from 50 to 0°C. As expected, the crystal structure reveals discrete, μ-Cl-bridged, dimeric molecules (Fig. 1, Tables 1–3). There are two independent, non-planar species $[(dtbpm)RhCl]_2$ in each asymmetric unit. The coordination geometry at all Rh centres is exactly planar; the maximum deviation from the plane is 0.03 Å. The four-membered RhPCP rings are equally planar. Their angles P–Rh–P are between 75.3 and 76.4° and fit well those of many other complexes with [M(dtbpm)] substructures (M = Rh, Ir, Ni, Pd, Pt) which we have studied by X-ray diffraction

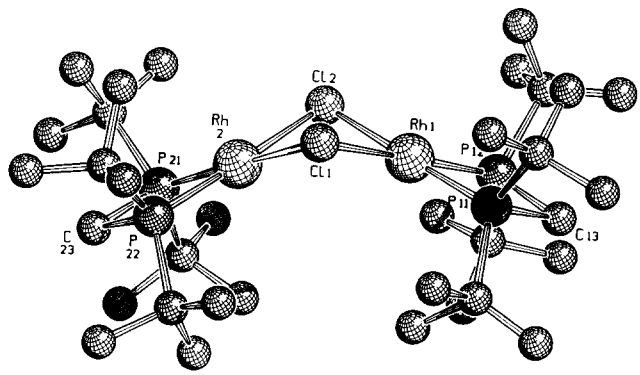

Fig. 1. Molecular structure of **10** in the crystal (only one of the two independent molecules is shown, hydrogens omitted for clarity).

Table 1
Crystallographic data and data collection for [(dtbpm)RhCl]$_2$ (**10**)

Molecular formula	$C_{34}H_{76}Cl_2P_4Rh_2$
Molecular weight	885.6
Crystal system	Monoclinic
Space group	$P2_1/c$
Crystal dimensions (mm)	0.2×0.3×0.4
a (pm)	1310.5(2)
b (pm)	1676.2(4)
c (pm)	3943.6(9)
β (°)	91.39(2)
V (nm^3)	8.660(5)
Z	8
$D_{calc.}$ (g cm^{-3})	1.358
Radiation	Cu Kα (λ = 1.5406 Å)
μ(Cu Kα) (cm^{-1})	90.54
F(000)	3712
Scan type	$\omega - \theta$
θ range (°)	5–55
Total No. of reflections	7512
No. of non-equivalent reflections ($I > 3\sigma(I)$)	5679
No. of parameters refined	418
$R = \Sigma \|\|F_o\| - \|F_c\|\| / \Sigma \|F_o\|$	0.084
$R_w = [\Sigma w(\|F_o\| - \|F_c\|)^2 / \Sigma w F_o^2]^{1/2}$	0.097, $w = 1/\sigma^2(F_o)$
Goodness of fit	5.816
Final max $\Delta\rho$ (e Å^{-3})	1.1 (disorder of ^{t}Bu groups)

[23]. The intra-ring valence angle at the methylene carbon is squeezed to values between 89.6 and 94.4°, which again are characteristic values for [M(dtbpm)] subunits.

The first structure determination of a dimeric, μ-Cl bridged rhodium (I) complex was reported by Dahl et al. [24] in 1961, and many structures have appeared since then. It was found that the Rh_2Cl_2 frame of $(CO)_4Rh_2Cl_2$ (Dahl's compound) is also not planar, but folded along the Cl–Cl axis, as shown schematically in **12**. The folding angle γ is defined as the dihedral angle between the coordination planes of the two Rh centres ($\gamma = 180°$ means planar, $\gamma < 180°$ means folded geometries).

Table 2
Relevant bond lengths (Å) and bond angles (°) of **10** (standard deviations in parentheses) [a]

Rh1–Cl1	2.436(2)/2.408(2)	Cl1–Rh1–Cl2	85.47(9)/85.52(8)
Rh1–Cl2	2.409(3)/2.421(2)	Cl1–Rh1–P11	99.10(9)/98.41(8)
Rh2–Cl1	2.429(2)/2.435(3)	Cl2–Rh1–P12	99.6(1)/100.24(9)
Rh2–Cl2	2.432(2)/2.419(3)	P11–Rh1–P12	75.8(1)/75.79(9)
Rh1–P11	2.163(3)/2.201(3)	Cl1–Rh–Cl2	85.14(8)/84.96(9)
Rh1–P12	2.180(3)/2.205(2)	Cl1–Rh2–P22	99.40(8)/99.83(9)
Rh2–P21	2.192(3)/2.186(3)	Cl2–Rh2–P21	99.10(9)/99.94(9)
Rh2–P22	2.202(2)/2.196(3)	P21–Rh2–P22	76.37(9)/75.3(1)
P11–C13	1.91(1)/1.907(9)	Rh1–Cl1–Rh2	84.55(7)/84.63(7)
P12–C13	1.88(1)/1.835(9)	Rh1–Cl2–Rh2	85.05(8)/84.69(7)
P21–C23	1.861(8)/1.836(9)	P11–C13–P12	89.6(5)/92.6(4)
P22–C23	1.891(9)/1.81(1)	P21–C23–P22	92.8(3)/94.4(5)

[a] The corresponding values of the first and second crystallographic independent molecules are separated by a solidus.

A comparison of folding angles γ for various μ-Cl-bridged rhodium dimers reveals that non-planar structures as in Dahl's compound ($\gamma = 124°$ [24]) are frequently found, as in, e.g., $(C_2H_4)_4Rh_2Cl_2$ ($\gamma = 124°$ [25]), $(CO)_2(PPhMe_2)_2Rh_2Cl_2$ ($\gamma = 123°$) [26] and $(dfepe)_2M_2Cl_2$ (M = Rh, Ir, $\gamma = 128°$) [27]. Planar geometries are represented by $(C_8H_{12})_2Rh_2Cl_2$ [28], $(PPh_3)_4Rh_2Cl_2$ [29], $(P^iPr_3)_4Rh_2Cl_2$ [30] and *trans*-$(C_8H_{14})_2(PH\{CH(SiMe_3)_2\}_2)Rh_2Cl_2$ [31]. For **10**, we find the largest value γ (134°) of all non-planar structures determined so far and, as a consequence, the intramolecular Rh–Rh distance of 3.26–3.27 Å is around 0.2 Å longer than in all other complexes where γ is below 130°. Intermolecular metal–metal interactions, as discussed by Dahl et al. for the case of $(CO)_4Rh_2Cl_2$, do not play any role for **10**, where the closest contacts between the Rh atoms of two independent molecules exceed 8 Å.

The question of intramolecular Rh–Rh interactions in folded systems and of their significance for adopting non-planar geometries has been addressed by Summerville and Hoffmann [32] by means of MO calculations of the Extended Hückel (EH) type. Their bonding and electronic structure analysis did not reveal any obvious orbital energy or overlap effects, to which a preference for either folded or planar structures of such μ-Cl-bridged dimers could be consistently traced back. We have also performed EH calculations for $(PH_3)_4Rh_2Cl_2$ and in particular for [(dhpm)RhCl]$_2$ (dhpm = $H_2PCH_2PH_2$, as a model for dtbpm) [20,33] and find the planar geometries ($\gamma = 180°$) to be lowest in energy in both systems. It only costs around 10 kJ mol^{-1} in energy, however, to fold these dimers by 40° to an angle of $\gamma = 140°$. This clearly indicates that even packing effects in the crystal will be sufficient to determine the actual amount of folding found in solid-state structures. This is also illustrated in Fig. 2(a), a space-filling representation of the two independent molecules of **10** in the crystal (hydrogens omitted); owing to the folding along the Cl–Cl axis, the gap between the bulky dtbpm groups becomes larger, providing enough space for "embedding" a second molecule of **10**. A space-filling representation of one molecule of **10** (Fig. 2(b)) shows that the experimentally determined folding angle of 134° still does not cause too close steric contacts between the two approaching pairs of *endo*-^{t}Bu groups of both (dtbpm)Rh subunits.

The Rh–Cl bonds of **10** (2.42 Å) are on average 0.04 Å longer than in comparable monomeric, square-planar rhodium(I) complexes [35]. The Rh–Cl distance (2.38 Å) of (dtbpm)RhCl(PMe_3), which we reported recently and which is formed quantitatively from **10** and PMe_3 [20], is also significantly shorter than those of **10**. Other μ-Cl-bridged complexes with long Rh–Cl bond dis-

Table 3
Atomic coordinates and equivalent isotropic thermal parameters of **10** (estimated standard deviations in parentheses) [a]

Atom	x / a	y / b	z / c	B (Å²)
Molecule 1				
Rh1	0.5045(2)	0.7774(1)	0.3681(1)	2.41(5)
Rh2	0.2983(2)	0.8870(1)	0.3712(1)	2.33(5)
Cl1	0.3854(5)	0.8252(3)	0.3243(1)	2.9(2)
Cl2	0.3582(5)	0.7724(3)	0.4038(1)	3.8(2)
P11	0.6433(5)	0.7791(4)	0.3395(1)	3.1(2)
P12	0.6214(6)	0.7340(3)	0.4038(1)	3.2(2)
P21	0.2176(6)	0.9504(3)	0.4111(1)	3.1(2)
P22	0.2365(5)	0.9932(3)	0.3451(1)	2.0(2)
C11	0.659(2)	0.707(1)	0.3034(6)	5.7(7)
C12	0.696(2)	0.881(1)	0.3238(6)	6.3(7)
C13	0.733(2)	0.743(1)	0.3751(5)	4.1(6)
C14	0.660(2)	0.795(1)	0.4432(6)	5.1(6)
C15	0.614(2)	0.622(1)	0.4178(6)	4.9(6)
C21	0.296(2)	0.995(1)	0.4487(5)	4.1(6)
C22	0.098(2)	0.906(1)	0.4286(5)	3.6(5)
C23	0.171(2)	1.034(1)	0.3836(5)	2.8(5)
C24	0.139(2)	0.980(1)	0.3111(5)	2.9(5)
C25	0.331(2)	1.073(1)	0.3305(5)	3.6(5)
C111	0.648(3)	0.628(2)	0.3137(8)	9(1)
C112	0.590(2)	0.723(2)	0.2741(7)	8.2(9)
C113	0.772(3)	0.708(2)	0.2900(9)	11(1)
C121	0.641(2)	0.942(2)	0.3471(8)	8.8(9)
C122	0.639(2)	0.902(2)	0.2917(7)	7.3(8)
C123	0.805(3)	0.887(2)	0.3219(9)	12(1)
C141	0.577(2)	0.799(1)	0.4671(6)	5.4(7)
C142	0.682(2)	0.877(1)	0.4317(7)	6.3(7)
C143	0.759(2)	0.765(2)	0.4596(7)	7.3(8)
C151	0.565(3)	0.614(2)	0.4528(8)	10(1)
C152	0.537(2)	0.580(2)	0.3951(7)	7.4(8)
C153	0.710(3)	0.580(2)	0.4205(8)	10(1)
C211	0.403(2)	1.002(1)	0.4377(6)	5.7(7)
C212	0.257(2)	1.077(2)	0.4595(7)	6.6(8)
C213	0.304(2)	0.935(2)	0.4792(7)	6.6(7)
C221	0.026(2)	0.889(1)	0.4012(6)	5.4(7)
C222	0.124(2)	0.826(1)	0.4457(6)	5.3(7)
C223	0.041(2)	0.958(1)	0.4553(6)	6.3(7)
C241	0.176(2)	0.989(1)	0.2753(6)	4.7(6)
C242	0.098(2)	0.896(1)	0.3127(6)	4.7(6)
C243	0.047(2)	1.032(1)	0.3144(6)	4.5(6)
C251	0.387(2)	1.045(1)	0.3019(6)	5.3(6)
C252	0.269(2)	1.152(1)	0.3192(5)	3.4(5)
C253	0.392(2)	1.097(1)	0.3609(6)	5.4(7)
Molecule 2				
Rh3	0.8052(2)	0.3537(1)	0.3756(1)	2.57(5)
Rh4	1.0113(2)	0.4622(1)	0.3817(1)	2.37(5)
Cl3	0.8911(5)	0.4154(3)	0.4234(1)	3.2(2)
Cl4	0.8640(5)	0.4673(3)	0.3436(1)	3.4(2)
P31	0.7163(6)	0.2904(3)	0.3359(1)	3.4(2)
P32	0.7434(5)	0.2486(3)	0.4017(1)	2.6(2)
P41	1.1287(6)	0.5060(4)	0.3480(1)	3.5(2)
P42	1.1525(5)	0.4615(3)	0.4128(1)	3.0(2)
C31	0.776(2)	0.245(1)	0.2977(6)	5.4(7)
C32	0.593(2)	0.340(1)	0.3174(6)	4.2(6)
C33	0.674(2)	0.206(1)	0.3649(5)	3.3(5)
C34	0.829(2)	0.167(1)	0.4179(5)	4.1(6)
C35	0.639(2)	0.263(1)	0.4369(6)	4.5(6)
C41	1.113(2)	0.617(1)	0.3347(6)	5.3(7)
C42	1.167(2)	0.444(1)	0.3100(6)	6.2(7)
C43	1.234(2)	0.496(1)	0.3794(5)	3.6(5)
C44	1.165(2)	0.532(1)	0.4506(6)	5.8(7)
C45	1.207(2)	0.360(1)	0.4262(6)	5.1(6)
C311	0.880(3)	0.217(2)	0.309(1)	15(1)
C312	0.725(3)	0.174(2)	0.283(1)	14(1)
C313	0.812(2)	0.299(2)	0.2716(7)	7.8(8)
C321	0.514(3)	0.286(2)	0.3036(9)	11(1)
C322	0.615(3)	0.402(2)	0.2892(9)	11(1)
C323	0.555(3)	0.386(2)	0.344(1)	16(2)
C341	0.885(2)	0.189(2)	0.4500(7)	7.1(8)
C342	0.913(3)	0.160(2)	0.3930(9)	11(1)
C343	0.785(3)	0.090(2)	0.420(1)	14(1)
C351	0.570(3)	0.200(2)	0.4367(8)	10(1)
C352	0.698(3)	0.279(2)	0.4707(8)	10(1)
C353	0.596(3)	0.351(2)	0.4343(9)	11(1)
C411	1.096(3)	0.662(2)	0.3632(9)	13(1)
C412	1.038(2)	0.632(2)	0.3067(7)	8.0(9)
C413	1.222(3)	0.643(2)	0.3198(9)	12(1)
C421	1.096(2)	0.464(2)	0.2795(8)	9.0(9)
C422	1.272(3)	0.465(2)	0.297(1)	15(1)
C423	1.149(3)	0.364(2)	0.3185(9)	12(1)
C441	1.082(2)	0.597(2)	0.4483(7)	7.8(8)
C442	1.135(2)	0.495(2)	0.4842(8)	10(1)
C443	1.262(3)	0.577(2)	0.4526(8)	11(1)
C451	1.144(2)	0.326(2)	0.4519(7)	7.5(8)
C452	1.322(3)	0.372(2)	0.4430(9)	11(1)
C453	1.209(3)	0.310(2)	0.3986(8)	9(1)

[a] Anisotropically refined atoms (Rh, P, Cl) are given in the form of the isotropic equivalent displacement parameter, defined as $(4/3)[a^2B(1,1)+b^2B(2,2)+c^2B(3,3)+ac(\cos\beta)B(1,3)]$.
All carbon atoms were refined isotropically.

tances are *trans*-$(C_8H_{14})_2(PH\{CH(SiMe_3)_2\}_2)Rh_2Cl_2$ (2.44 Å, Rh–Cl *trans* to the phosphine ligands) [31], $(P^iPr_3)_4Rh_2Cl_2$ (2.43 Å) [30] and *cis*-$(CO)_2(PPhMe_2)_2Rh_2Cl_2$ (2.43 Å, Rh–Cl *trans* to the phosphine ligands) [26]. Rh–Cl bonds *trans* to olefin or carbonyl ligands are shorter, typical examples being $(COD)_2Rh_2Cl_2$ with 2.38 Å and $(CO)_4Rh_2Cl_2$ with 2.35 Å. Interestingly, the dissociation of the dimer $(C_8H_{14})_2(PH\{CH(SiMe_3)_2\}_2)Rh_2Cl_2$ in solution has been explained on the basis of its elongated Rh–Cl linkage *trans* to the phosphines [31], and for Werner's compound $(P^iPr_3)_4Rh_2Cl_2$ a molecular weight determination [36] has been interpreted as proof of reactive, monomeric 14-electron units $[(P^iPr_3)_2RhCl]$ in solution. For these tricoordinate (T-shaped) species the P–Rh–P angle of 105° of the dimer will, of course, open up after dissociation in order to allow for a more favourable *trans* position of the two bulky phosphines in the monomer. In accord with these observations, the large Rh–Cl distances of the dimer **10** are also reflected in its facile and complete dissociation into (probably solvent-stabilized) [(dtbpm)RhCl] monomers in solution [20]. It should be mentioned that our previous EH MO calculations for the simplified dimer models $(PH_3)_4Rh_2Cl_2$ and $[(dhpm)RhCl]_2$ had predicted [20] that a deviation of

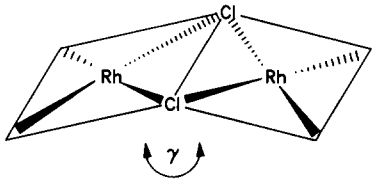

12

the P–Rh–P angles to values above or below the ideal value of 90° should cause a weakening of the Rh–μ-Cl bonds. For **10** with its chelate ligands and its smaller P–Rh–P angles of only 75°, this theoretical conclusion is confirmed experimentally by the present X-ray structure determination and fits nicely the observations made for $(P^iPr_3)_4Rh_2Cl_2$ [30], where the P–Rh–P angles (105°) exceed the optimum 90° by approximately the same amount of ca. 15°.

Owing to the high P-basicity of the dtbpm ligands, the Rh–P bond lengths of **10** are slightly shorter than in other typical Rh complexes with monodentate phosphine ligands [35], despite the steric bulk of the ^{t}Bu substituents, which would tend to stretch the metal to phosphorus distances. Short Rh–P bonds have been found recently also for $(dfepe)_2Rh_2Cl_2$ (2.15 Å) with its very electronegative phosphine ligand [27].

Having established the solid-state structure of the dimer $[(dtbpm)RhCl]_2$ and its facile dissociation in solution, it seemed was desirable to test the catalytic potential of the (solvated) 14-electron monomer [(dtbpm)RhCl]. We have already reported [20] that the dimer $[(dtbpm)RhCl]_2$ (**10**) catalyses the trimerization of certain alkynes (e.g. of but-2-yne to hexamethylbenzene and of bis(carbomethoxy)acetylene to hexakis(carbomethoxy)benzene), and that it slowly hydrogenates benzene to cyclohexane (room temperature 1 bar). Compound **10** is also an efficient catalyst for the cyclization of pentyne-4-carboxylic acid to tetrahydro-5-methylene-2-furanone, comparable to the related dimer $[(dcpe)RhCl]_2$ reported by Marder and coworkers [22], for which the dissociative formation of monomeric [(dcpe)RhCl] units has also been assumed.

We have now found that dimer **10** can function as a catalyst in homogeneous hydrosilylation reactions of alkenes and alkynes. With hex-1-ene as an olefinic test substrate and either triethylsilane or triethoxysilane (0.1 mol% **10** as catalyst, olefin:silane ratio = 1:1, 40°C, no solvent, argon atmosphere), the anti-Markownikov products triethyl-*n*-hexylsilane and triethoxy-*n*-hexylsilane were formed in 80% (turnover 100 h^{-1}) and 58% (turnover 75 h^{-1}) isolated yield, respectively. As a side-reaction, isomerization of hex-1-ene accompanies hydrosilylation; an amount of ca. 10% of internal alkenes is not hydrosilylated under the reaction conditions. In relation to other known rhodium hydrosilylation catalysts, $[(dtbpm)RhCl]_2$ is of comparable activity, slightly less efficient than the recently reported dimer di-μ-chloro(η^2-methylenecyclopropane)dirhodium [37]. Therefore, no efforts were made to optimize alkene hydrosilylation by **10** or by derivatives of this compound at this point. Instead, we decided to focus on hydrosilylation catalysis of alkynes, because here some early experiments and observations seemed to indicate high catalytic activity for properly

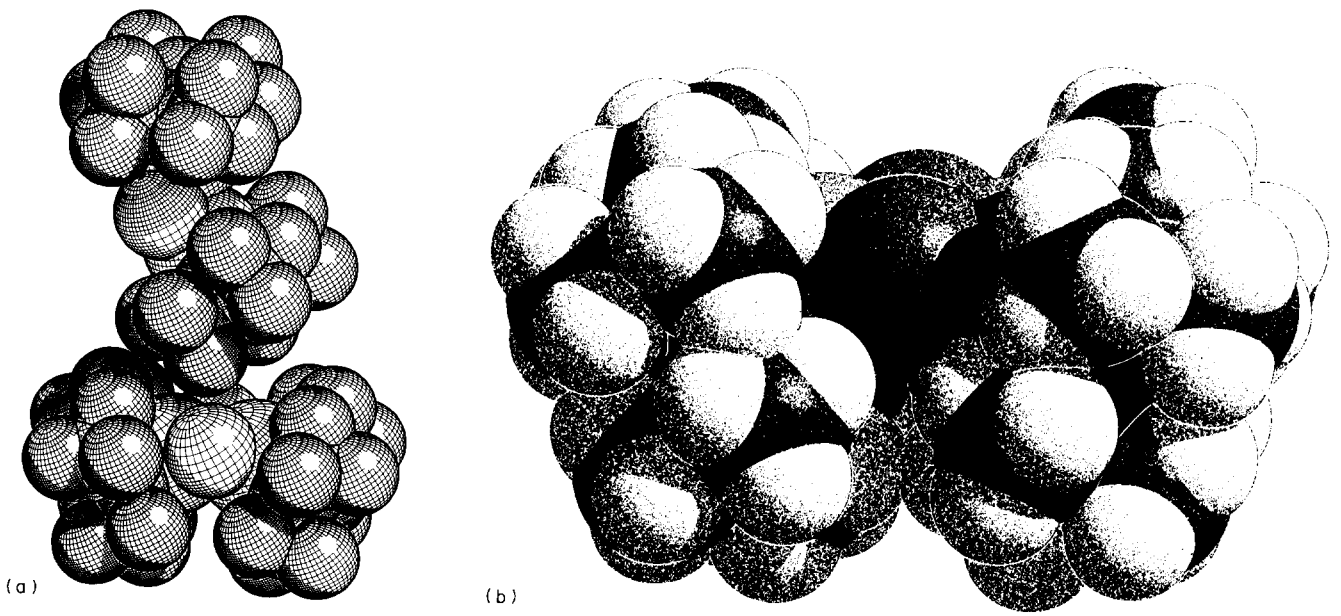

Fig. 2. (a) Space-filling representation of the two independent molecules of **10** in the crystal (hydrogens omitted). (b) Space-filling representation of one molecule of **10**, with hydrogens added (CPK, SCHAKAL [34]).

Table 4
Homogeneous hydrosilylation of but-2-yne with $HSi(OEt_3)$ to (*E*)-2-triethoxysilyl-but-2-ene at room temperature

Catalyst	Catalyst concentration (mol%)	Reaction time (h)	Yield (%) [a]	Turnover (pe 30 min)
10	0.1	5 [b]	59 [c]	85
10 + 2 PPh_3	0.1	0.5	100	1000
10 + 2 PPh_3	0.05	0.5	85	1480
11	0.2	3	–	–
13a	0.4	0.5	100	250
13a	0.1	0.5	93 [d]	1000
14	0.4	0.5	100	250
14	0.1	0.5	87 [e]	1000

[a] From NMR data.
[b] At 40°C.
[c] Plus 27% *trans*-addition product, 16% hexamethylbenzene.
[d] Plus 7% *trans*-addition product.
[e] Plus 13% *trans*-addition product.

modified catalyst systems based on **10**. This will be discussed in detail in the next section, before we turn to non-Harrod–Chalk-type hydrosilylation catalysis of alkynes via alkyne insertion into Rh–Si bonds.

2.1. Alkyne hydrosilylation by [(dtbpm)RhCl]$_2$ (10) without and with added PPh_3

But-2-yne and triethoxysilane were chosen as the standard system (molar ratio 1 : 1) to investigate alkyne hydrosilylation reactions for different catalysts under comparable conditions (no solvent, neat mixture of reactants and catalyst, argon atmosphere; see Table 4). As our simplest catalyst precursor, we first tested the dimer [(dtbpm)RhCl]$_2$ (**10**).

With a catalyst concentration of 0.1 mol%, the reaction of triethoxysilane and the alkyne takes place readily at 40°C. After 5 h, 86% of the silane has disappeared. In addition to 16% of hexamethylbenzene, the trimerization product of but-2-yne (see above), NMR analysis shows the formation of the product of silane *cis*-addition to but-2-yne, (*E*)-2-triethoxysilylbut-2-ene, in 59% yield. A second triethoxysilyl-substituted alkene is produced in 27% yield, to which we assign the structure of the *trans*-isomer (*Z*)-2-triethoxysilylbut-2-ene from ^1H NMR. The hydrosilylation turnover number for **10** as a catalyst at 40°C is calculated to be at least 170 h^{-1}. Dimer **10** is therefore catalytically active under distinctly milder conditions than, e.g., Speier's catalyst [1,2]; its disadvantage lies in its lack of *cis/trans* selectivity and its trimerization activity, at least for our standard system of but-2-yne and triethoxysilane.

It is possible, however, to improve the catalyst performance of dimer **10** drastically and to create a highly active and also very selective system by adding 2 mol of triphenylphosphine per mol of [(dtbpm)RhCl]$_2$ (Eq. (1)).

$$H_3C{-}C{\equiv}C{-}CH_3 + HSi(OEt)_3 \xrightarrow{\mathbf{10}+2\ PPh_3} \underset{H}{\overset{CH_3}{\diagdown}}C{=}C\underset{Si(OEt)_3}{\overset{CH_3}{\diagup}} \quad (1)$$

(*E*)-2-triethoxysilylbut-2-ene

According to Eq. (1), we now find exclusive *cis*-addition of the silane and quantitative formation of (*E*)-2-triethoxysilylbut-2-ene under the same reaction conditions as described above (Table 4). Only 1% trimerization product is detected. For a concentration of 0.1 mol% of dimer **10** with 0.2 mol% of PPh_3 added (amounting to the same rhodium concentration as applied for **10** alone), the reaction is already complete after 0.5 h, which corresponds to a minimum turnover number of 1000 per 30 min. When the amount of catalyst is reduced by 50% (i.e. to 0.05 mol% of **10** + 0.1 mol% of PPh_3), 85% of the starting material is converted into (*E*)-2-triethoxysilylbut-2-ene after a 0.5 h period, which corresponds to a turnover number of 1480 per 30 min. The improvement for both reactivity and selectivity on adding triphenylphosphine to **10** is remarkable and needs to be discussed. From earlier studies [20], we know that the addition of monodentate ligands L (L = CO, PMe_3, PPh_3, PCy_3, pyridine, acrylonitrile) to the chloro-bridged dimer **10** leads to a facile splitting of the μ-Cl bridges and allows to prepare the mononuclear, square-planar complexes (dtbpm)RhCl(L) (**9**, M = Rh, X = Cl). For L = PPh_3, PCy_3, pyridine and acrylonitrile these compounds have been shown to dissociate their monodentate ligands in solution, the dissociation equilibria being a function of the donor strength, the acceptor character and the steric demand of L. Thus, the addition of PPh_3 to [(dtbpm)RhCl]$_2$ is equivalent to an in situ preparation of the complex (dtbpm)RhCl(PPh_3) [20] as the precatalyst, which in turn is capable of delivering the 14-electron fragment [(dtbpm)RhCl] (**8**, M = Rh, X = Cl) as the active species to promote hydrosilylation. Without PPh_3 added, dimer **10** provides [(dtbpm)RhCl] by direct dissociation. Hence we consider it reasonable to assume (Scheme 1) that for both catalytic systems, **10** and **10** + PPh_3, this unsaturated intermediate initiates hydrosilylation by oxidative addition of the silane Si–H bond to the metal centre, yielding **A** (16 valence electrons), followed by subsequent insertion of the alkyne into the Rh–H bond to give **B** (16 valence electrons) and finally by reductive elimination of the vinylsilane and regeneration of [(dtbpm)RhCl], in accord with the general formulation of the Harrod–Chalk picture [4].

As an alternative to Scheme 1, one might assume that the direct oxidative silane addition to the intact dimer **10** or, for the **10** + PPh_3 catalyst system, to the

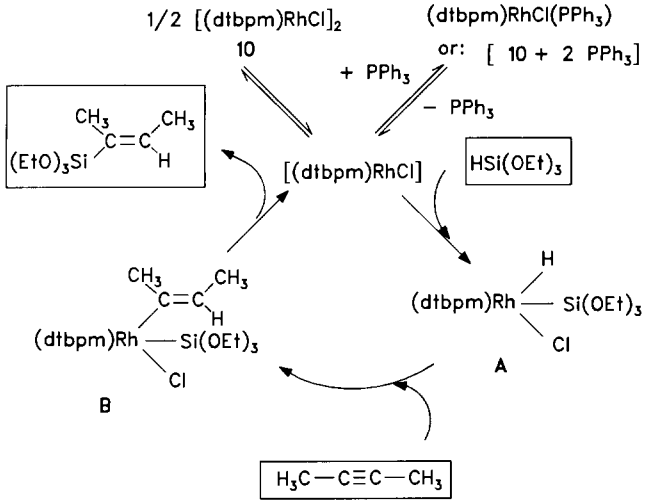

Scheme 1.

preformed complex (dtbpm)RhCl(PPh_3), is the first step of the catalytic cycle. This would somehow explain the difference in catalyst reactivity for the two systems. It is experimentally possible to exclude this alternative and to establish that the involvement of the tricoordinate 14-electron fragment [(dtbpm)RhCl] is indeed a realistic assumption. The necessary test experiment relies on our previous finding that, different from the phosphine complex (dtbpm)RhCl(PPh_3), its PMe_3 analogue (dtbpm)RhCl(PMe_3) (**11**) [20] does *not* dissociate in solution. As a consequence, this complex itself or the addition of PMe_3 instead of PPh_3 as a cocatalyst for dimer **10** should inhibit the dissociative generation of [(dtbpm)RhCl] and should thus suppress hydrosilylation if the formation of [(dtbpm)RhCl] is required. If, on the other hand, direct addition to the 16-electron Rh centres of **10** or (dtbpm)RhCl(PPh_3) is the initiating step of the catalytic cycle, then **11** with its more electron-rich metal centre should also be a catalyst. We find this not to be the case. Under otherwise identical reaction conditions, the replacement of PPh_3 by PMe_3 blocks hydrosilylation by $[(dtbpm)RhCl]_2$ completely, supporting Scheme 1.

In the absence of kinetic data for the catalytic reaction, we are unable to determine unequivocally the origin of catalyst improvement by PPh_3 compared with the dimer **10** alone. It is conceivable that five-coordinate species such as **A** and/or **B** in Scheme 1, the precise stereochemistry of which is unknown (see structures **4–6**; L = Cl, $Si(OEt)_3$, H) are stabilized by reversible PPh_3 coordination within the catalytic cycle, thus improving catalyst reactivity and selectivity by blocking, e.g., decomposition or undesired side-reactions. More detailed studies, varying the reaction conditions, substrates and the added phosphine (or coligand in general), will be necessary to gain further insight. These studies are under way.

2.2. Dissociation behaviour of (dtbpm)RhCl(PPh_3)

Given the role of PPh_3 in the catalytic reaction of Eq. (1), we decided to examine more closely the dissociation behaviour of (dtbpm)RhCl(PPh_3). Similarly to the pyridine complex (dtbpm)RhCl(C_5H_5N) [20], ^{31}P and ^{1}H NMR spectroscopy allow one to study the temperature dependence of PPh_3 dissociation for this complex and to determine its dissociation constant. Fig. 3 displays the ^{31}P NMR spectra of a C_6D_6 solution of (dtbpm)RhCl(PPh_3) at 5, 25 and 70°C.

As is evident from the growing peak intensities for free PPh_3 and the diminished intensities for P_A, P_B and P_C of (dtbpm)RhCl(PPh_3), the extent of PPh_3 dissociation increases with increasing temperature. Accompanying the appearance of free PPh_3, the synchronous increase of a doublet signal is observed, which is identical with that measured for a solution of the pure dimer $[(dtbpm)RhCl]_2$ (**10**) in C_6D_6. As already mentioned, molecular weight determinations for these solutions were in agreement with practically complete dissociation of $[(dtbpm)RhCl]_2$ into (presumably solvated) monomers [(dtbpm)RhCl]. The dissociation equilibrium of (dtbpm)RhCl(PPh_3) should thus be described by Eq. (2).

$$(dtbpm)RhCl(PPh_3) \rightleftharpoons [(dtbpm)RhCl]_{solv.} + PPh_3 \quad (2)$$

If for the moment we disregard the molecular weight experiments, an alternative formulation of the PPh_3 dissociation equilibrium would involve the dimer **10** instead of monomeric species, according to Eq. (3)).

$$2\,(dtbpm)RhCl(PPh_3) \rightleftharpoons [(dtbpm)RhCl]_2 + 2\,PPh_3 \quad (3)$$

Obviously, both possibilities lead to different expressions for the respective equilibrium constants K_m (for Eq. (2)) and K_d (for Eq. (3)). In a rewritten form, these expressions are given in Eqs. (4) and (5) ([E] = equilibrium concentration of educt (dtbpm)RhCl(PPh_3), $[PPh_3]$ = equilibrium concentration of PPh_3, [P] = equilibrium concentration of product [(dtbpm)RhCl] in Eq. (2) or $[(dtbpm)RhCl]_2$ in Eq. (3)).

$$[P] = K_m[E]/[PPh_3] \quad (4)$$

$$[P] = K_d([E]/[PPh_3])^2 \quad (5)$$

An experimental determination of $[P] = f([E]/[PPh_3])$ at constant T should thus allow one to differentiate between the equilibria of Eqs. (2) and (3) and, if a linear dependence between [P] and $[E]/[PPh_3]$ is found, to gather further evidence for the intermediacy of (solvated) [(dtbpm)RhCl] as an intermediate in the catalytic cycle in Scheme 1.

Quantitative ^{31}P NMR spectroscopy was employed to determine $[P] = f([E]/[PPh_3])$ for ten samples

(C_6D_6) with different initial concentration ratios of dimer **10** and PPh_3. The equilibrium concentrations of all three P-containing species (see Fig. 3) were then determined at 70°C by careful peak integration (for details of the ^{31}P measurements, see Experimental). Fig. 4 shows [P] plotted against [E]/[PPh_3] as expected

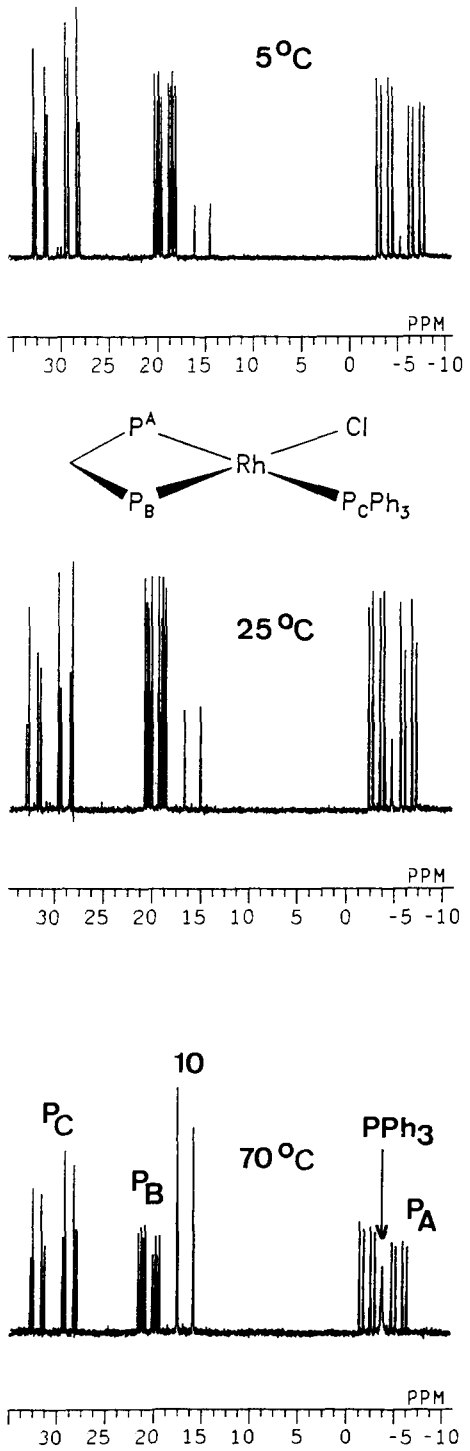

Fig. 3. ^{31}P NMR spectra of (dtbpm)RhCl(PPh_3) in C_6D_6 at three different temperatures.

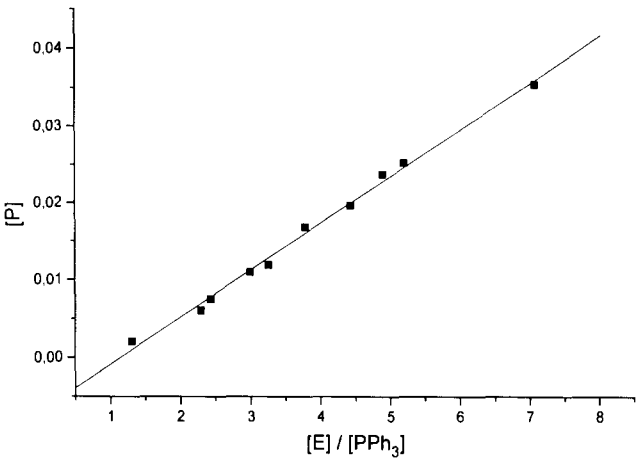

Fig. 4. Plot of measured values (^{31}P NMR) of [P] against [E]/[PPh_3] (70°C) showing the linear relation expected from Eq. (2).

for the dissociation equilibrium of Eq. (2) with monomer [(dtbpm)RhCl] involved.

The data fit a linear relationship between [P] and [E]/[PPh_3], as expected for Eq. (2) (linear regression analysis yields a correlation coefficient $r = 0.998$). In contrast, an analogous plot of [P] vs. ([E]/[PPh_3])^2 leads to a much worse fit, with most data points deviating significantly from the best straight line and linear regression gives an r value of only 0.978. These results, in addition to the molecular weight data, the solid-state structure and the catalytic properties of [(dtbpm)RhCl]$_2$, lend further credit to our conclusion that weakly solvated monomeric units [(dtbpm)RhCl] are easily generated in solution from either [(dtbpm)-RhCl]$_2$ or from (dtbpm)RhCl(L) complexes **9** with weakly coordinating ligands L, and that these reactive intermediates play a dominant role in the catalytic hydrosilylation described above.

From Fig. 4, the equilibrium constant for the dissociation of (dtbpm)RhCl(PPh_3) at 70°C (Eq. (2)) can be read off as $K_m^{343} = 6.3 \times 10^{-3}$ mol l^{-1}. This value was cross-checked by determining K_m independently by ^1H NMR spectroscopy at the same temperature. The value obtained this way is $K_m^{343} = 5.4 \times 10^{-3}$ mol l^{-1}, in good agreement with the ^{31}P-based value. We can compare these values with the PPh_3 dissociation constant of the Wilkinson complex (PPh_3)$_3$RhCl. From kinetic investigations by Halpern and Wong [38] (rate of PPh_3 dissociation = 0.7 s^{-1}) and from flash-photolysis experiments by Wink and Ford [39] (rate of PPh_3 recoordination = 3×10^{-6} l mol^{-1} s^{-1}) an approximate K of 2.3×10^{-7} mol l^{-1} is calculated. This value is three orders of magnitude below our K_m^{298} value (3.3×10^{-4} mol l^{-1}) for PPh_3 dissociation (Eq. (2)) from (dtbpm)RhCl(PPh_3), indicating a more pronounced dissociation tendency for the latter, which is certainly understandable on steric grounds. Even for the sterically crowded square-planar rhodium trisphosphine hy-

Table 5
Dissociation of PPh_3 from (dtbpm)RhCl(PPh_3): determination of equilibrium constants (^1H NMR, $[E]_0$ (dtbpm)RhCl(PPh_3) in C_6D_6 = 0.065 mol l^{-1})

T (°C)	Relative concentration (mol l^{-1})			Equilibrium constant, K_m (mol l^{-1})
	[E]	[P]	$[PPh_3]=[P]$	
10	0.0621	0.00289	0.00289	1.35×10^{-4}
25	0.0605	0.00451	0.00451	3.35×10^{-4}
40	0.0575	0.00746	0.00746	9.68×10^{-4}
55	0.0539	0.0111	0.0111	2.29×10^{-3}
70	0.0488	0.0162	0.0162	5.40×10^{-3}

dride complex $(DBP)_3RhH$ (DBP = 5-phenyl-5*H*-dibenzophosphole) [40], a dissociation constant of 8.9×10^{-5} mol l^{-1}, still smaller than our value for (dtbpm)RhCl(PPh_3), has been reported. Parenthetically we mention that (dppm)RhCl(PPh_3) with phenyl substituents instead of ^{t}Bu groups [41] does not dissociate its PPh_3 ligand.

Utilizing ^1H NMR, it was also possible to work out the thermodynamic parameters for the dissociation equilibrium of (dtbpm)RhCl(PPh_3) in Eq. (2). For a solution of the complex in C_6D_6, a temperature series was measured in the range 10–70°C and the relative concentrations were determined by integration of the ^{t}Bu and CH_2 signals of (dtbpm)RhCl(PPh_3) and of (solvated) [(dtbpm)RhCl] (for details, see Experimental). Table 5 collects the data (average values, each obtained from four independent measurements), and Fig. 5 is the associated plot of ln $K=f(T^{-1})$, from which we derive values of $\Delta H = 51\pm3$ kJ mol^{-1} and $\Delta S = 104\pm9$ J mol^{-1} K^{-1}.

We do not know of any comparable thermochemical ΔH and ΔS data for sufficiently similar compounds and their ligand dissociation equilibria, but ΔH seems to fall within the reasonable range of ligand binding energies [42] and the sign and magnitude of ΔS are as expected on grounds of Eq. (2). Again, more data are required in order to tailor reactivity patterns properly.

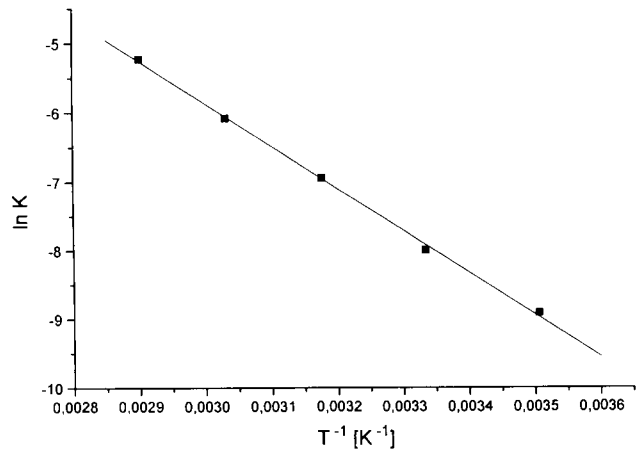

Fig. 5. Experimental ln K values (^1H NMR) for PPh_3 dissociation (Eq. (2)) from (dtbpm)RhCl(PPh_3) as a function of T^{-1} ($r=0.999$).

2.3. Synthesis of and alkyne hydrosilylation catalysis by alkyl rhodium complexes: hydrosilylation by alkyne insertion into Rh–Si bonds

The ready availability of tetracoordinate, chloro-substituted Rh^I complexes **9** [20] provided simple access to a series of square-planar Rh^I alkyl complexes (dtbpm)RhR(L) (**13a–c**).

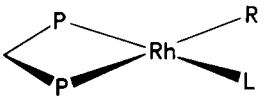

13

13a: L=PMe_3, R=Me

13b: L=PPh_3, R=Me

13c: L=CO, R=Np

The new compounds were characterized by ^1H, ^{31}P and ^{13}C NMR, IR and mass spectrometry and by elemental analysis. For the neopentyl carbonyl system **13c** a structure determination by X-ray crystallography is available [43], which will be reported separately. Here we shall focus on **13a**, which can be synthesized in good yield by reacting a slurry of the chloro complex **11** in hexane with a slight excess of methyllithium in diethyl ether at 0°C (Eq. (6)).

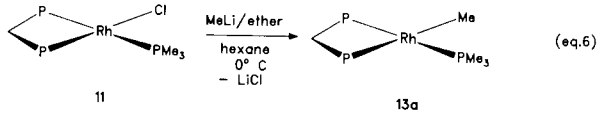

11 13a (eq.6)

Our impetus to test alkyl complex **13a** in alkyne hydrosilylation reactions was triggered by a paper by Thorn and Harlow [44], who showed that the oxidative addition of the silane Si–H bond of Ph_3SiH to the phosphine-rich Rh^I alkyl complex $(PMe_3)_{3,4}RhMe$ leads to an intermediate with adjacent silyl, alkyl and hydrido ligands at the metal centre (postulated for Rh, isolated for Ir), which then rapidly eliminates methane, giving the stable, structurally characterized Rh–silyl complex $(PMe_3)_3Rh(SiPh_3)$. For iridium, a related observation has been made recently by Aizenberg and Milstein [45]. Most interestingly however, Thorn and Harlow's complex $(PMe_3)_3Rh(SiPh_3)$ inserts ethylene into the Rh–Si bond, as evidenced by the (non-catalytic) formation of vinylsilane. Although the number of known Rh^I alkyl or aryl complexes is about 20, to our knowledge their propensity to catalyse hydrosilylation reactions has not been investigated, and insertion reactions into transition metal–silicon bonds are generally rare [46,47]. We reasoned that very electron-rich systems such as **13a**, where phosphine dissociation steps are even more unlikely than for the non-dissociative (see above) chloro complex **11**, might give us the opportunity to generate well defined Rh^I–silyl intermediates by direct oxidative Si–H addition plus irreversible

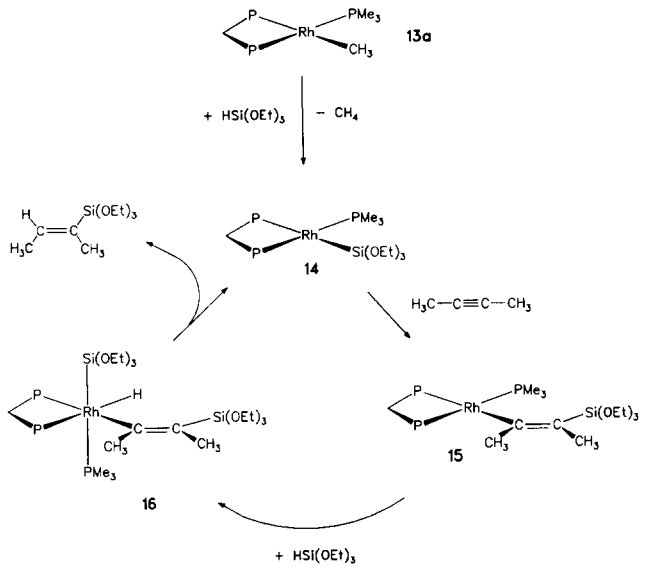

Scheme 2.

methane elimination, and to study their behaviour towards alkynes under catalysis conditions.

In contrast to its unreactive chloro precursor **11**, the methyl complex **13a** indeed catalyses the hydrosilylation of but-2-yne with triethoxysilane very efficiently and with high *cis*-stereoselectivity (standard conditions as above, 25°C, see Table 4). After a reaction time of 0.5 h (catalyst concentration 0.4 and 0.1 mol%), product formation is complete, as judged from NMR. The turnover number of 1000 per 30 min again has to be considered as a lower limit due to the first NMR spectrum taken after 30 min. The mechanism which we assume on the basis of the available information is presented in Scheme 2.

The formation of the silyl complex **14** by oxidative addition of $HSi(OEt)_3$ to **13a** and by subsequent elimination of methane is the key step in this scenario, creating **14** as the catalysis-carrying intermediate. Its generation we assume to be followed by (i) insertion of but-2-yne into the Rh–Si bond of **14** to give the Rh^{I} vinyl intermediate **15**, (ii) oxidative addition of another silane molecule to give the Rh^{III} complex **16** (note that **15** is a close structural analogue of **13a** and hence should display similar reactivity towards $HSi(OEt)_3$), and finally (iii) reductive elimination of the organic product (*E*)-2-triethoxysilylbut-2-ene from **16**. This last step regenerates **14**.

Our postulate of the catalytic cycle in Scheme 2, involving direct alkyne insertion into a Rh–Si bond of a Rh^{I} silyl complex rather than obeying the standard rules of Harrod–Chalk-type hydrosilylations, is supported by the following experimental findings. Most important, we were able to achieve the **13a** to **14** transformation in a separate, stoichiometric reaction and to isolate and characterize fully the silyl complex (dtbpm)Rh[$Si(OEt)_3$](PMe_3). Compound **14** can be prepared in 80–90% yield by reacting (dtbpm)RhMe(PMe_3) (**13a**) at −10°C with a slight excess of $HSi(OEt)_3$ in pentane. The orange solution of **13a** turns red immediately on silane addition, and the product (dtbpm)Rh[$Si(OEt)_3$](PMe_3) can be isolated as a red, crystalline material at −30°C. Compound **14** is rather sensitive, unstable in air and above room temperature. It is fully characterized by ^{1}H, ^{31}P and ^{13}C NMR spectroscopy, elemental analysis and X-ray diffraction, the results of which will be described below. If our picture of Scheme 2 holds, then **14** must of course catalyse hydrosilylation at least as well as its precursor in Scheme 2, **13a**. This was verified (Table 4), the yield, selectivity and turnover number being identical with those in the experiment with (dtbpm)RhMe(PMe_3) as a precatalyst. When the amount of (dtbpm)Rh[$Si(OEt)_3$](PMe_3) is reduced to 0.1 mol%, still 87% of (*E*)-2-triethoxysilylbut-2-ene and 13% of the *trans*-addition product are formed within 30 min, corresponding to a minimum turnover number of 1000 per 30 min at 25°C. Completion of the catalytic reactions is visible by a colour change from yellow to red, the colour of compound **14**, remaining after consumption of the substrates.

As a further test, we also ran a stoichiometric reaction (NMR-scale experiment) between **14** in solution and a stoichiometric amount of a 1:1 mixture of but-2-yne and triethoxysilane. As expected, the corresponding amount of (*E*)-2-triethoxysilyl but-2-ene was formed rapidly and ^{1}H NMR showed **14** to be still present.

We feel that these results are in good agreement with Scheme 2 for our catalytic alkyne hydrosilylation system. Further support, in particular for the insertion step of alkynes into the Rh–Si bond of **14**, will be presented after the structure description of the silyl complex.

2.4. Crystal and molecular structure of (dtbpm)Rh[Si(OEt)$_3$](PMe$_3$) (14)

Crystals of (dtbpm)Rh[$Si(OEt)_3$](PMe_3), suitable for X-ray diffraction (−70°C), were grown from a pentane solution at −30°C (Table 6). A structural representation of a molecule of **14** is shown in Fig. 6 and relevant bond distances, bond angles and fractional atomic coordinates are presented in Tables 7 and 8.

Despite appreciable steric crowding, the coordination geometry around Rh is precisely planar. The (dtbpm)Rh four-membered RhPCP ring is also planar, the P1–Rh–P3 angle being 74.4°. The steric demand of the ^{t}Bu groups is indicated by a comparison of P1–Rh–Si and P2–Rh–P3 bond angles. Repulsion between the PMe_3 ligand and its neighbouring ^{t}Bu substituents at P3 causes a widening of the P2–Rh–P3 angle to 102.7° as compared with 95.4° for P1–Rh–Si.

Table 6
Crystallographic data and data collection for (dtbpm)Rh[Si(OEt)$_3$](PMe$_3$) (**14**)

Molecular formula	$C_{26}H_{62}O_3P_3RhSi$
Molecular weight	646.7
Crystal system	Orthorhombic
Space group	$P2_12_12_1$
Crystal dimensions (mm)	0.2×0.25×0.5
a (pm)	1096.8(1)
b (pm)	1216.4(1)
c (pm)	2553.2(1)
V (nm^3)	3.406(1)
Z	4
$D_{calc.}$ (g cm^{-3})	1.261
μ (Mo Kα) (mm^{-1})	0.700
F(000)	1384
Scan type	ω
θ range (°)	3–27
Reflections measured	7876
Reflections observed	6335 [$F_o > 4\sigma(F_o)$]
No. of parameters refined	302
R_1 [a]	0.0470
wR_2 [b]	0.132
Flack parameter	0.01(4)
Goodness of fit	0.926
Final max $\Delta\rho$ (e Å^{-3})	0.612

[a] $R_1 = \Sigma \| F_o | - | F_c \| / \Sigma | F_o |$; ($F > 4\sigma(F)$).
[b] $wR_2 = [\Sigma w(|F_o|^2 - |F_c|^2)^2 / \Sigma w(F_o^2)^2]^{1/2}$.

A similar in-plane distortion had been found for (dtbpm)RhCl(PMe$_3$) earlier [20]. The atoms Si, O1/2, C2/3 and C6/7 all are close to being coplanar; the oxygen of the third OEt group is pointing towards the adjacent ^{t}Bu$_2$P unit, lying within the coordination plane, bisecting the ^{t}Bu–P1–^{t}Bu angle. This orientation causes the Rh–Si–O3 angle to be smaller (114.3°) than the two other Rh–Si–O angles (Rh–Si–O1, 119.3°; Rh–Si–O2, 119.0°). The O1–Si–O2 angle (93.6°) is smaller than the O3–Si–O1 (103.4°) and O3–Si–O2 angles (104.2°). All Si–O bond lengths are equal within experimental error (1.65 Å). The pronounced *trans* effect of the silyl ligand is reflected in a

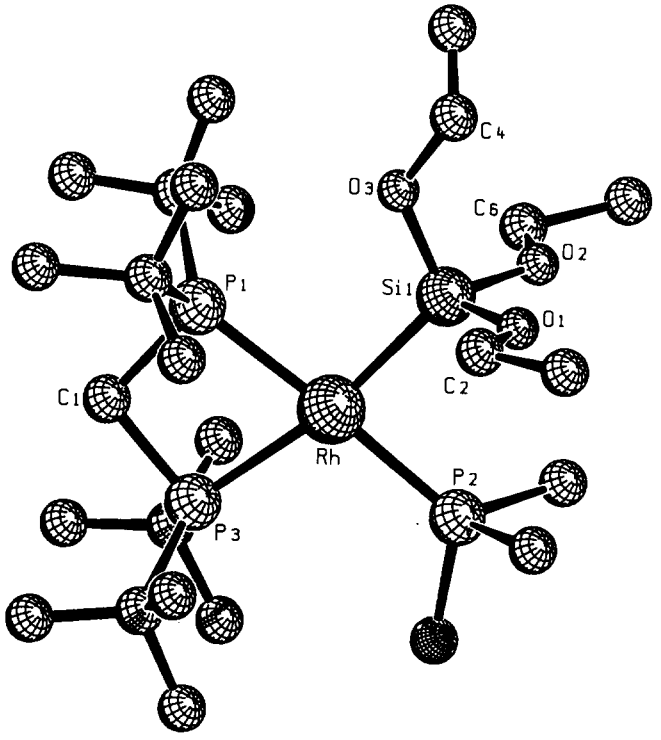

Fig. 6. Molecular structure of **14** (hydrogens omitted for clarity).

Table 7
Relevant bond lengths (Å) and bond angles (°) of **14** (standard deviations in parentheses)

Rh–P2	2.277(2)	P2–Rh–P1	176.76(6)	O1–Si–O2	93.6(2)
Rh–P1	2.315(1)	P2–Rh–Si	87.50(7)	O3–Si–O1	103.4(4)
Rh–P3	2.399(2)	P1–Rh–Si	95.37(5)	O3–Si–O2	104.2(4)
Rh–Si	2.325(2)	P2–Rh–P3	102.75(6)		
P1–C1	1.867(5)	P1–Rh–P3	74.39(5)		
P3–C1	1.868(5)	Si–Rh–P3	169.73(5)		
Si–O1	1.660(5)	O3–Si–Rh	114.3(2)		
Si–O2	1.657(4)	O2–Si–Rh	119.0(2)		
Si–O3	1.645(6)	O1–Si–Rh	119.3(3)		

Table 8
Atomic coordinates and equivalent isotropic displacement parameters (Å^2 × 10^2) of **14**

Atom	x/a	y/b	z/c	U(eq.)
Rh	−0.8180(1)	−0.0319(1)	−0.8820(1)	4.7(1)
P1	−0.9800(1)	−0.1418(1)	−0.8568(1)	4.3(1)
P2	−0.6533(2)	0.0737(2)	−0.9024(1)	8.2(1)
P3	−0.7321(1)	−0.1704(1)	−0.8261(1)	5.1(1)
Si	−0.9336(2)	0.0849(1)	−0.9342(1)	5.0(1)
O1	−0.9302(7)	0.2192(4)	−0.9228(2)	9.6(2)
O2	−0.8971(5)	0.0990(4)	−0.9968(2)	7.0(1)
O3	−1.0801(5)	0.0563(5)	−0.9350(3)	12.5(3)
C1	−0.8848(5)	−0.2344(4)	−0.8152(2)	4.8(1)
C2	−0.971(1)	0.2643(6)	−0.8746(4)	12.5(5)
C3	−0.962(1)	0.3878(7)	−0.8784(4)	17.0(7)
C4	−1.169(1)	0.128(1)	−0.9579(9)	19.0(9)
C5	−1.245(1)	0.088(1)	−0.9905(7)	17.2(8)
C6	−0.8860(9)	0.0080(7)	−1.0307(3)	8.4(2)
C7	−0.8577(9)	0.057(1)	−1.0860(3)	10.3(3)
C11	−1.0988(6)	−0.0880(5)	−0.8083(2)	5.8(1)
C12	−1.0595(6)	−0.2390(5)	−0.9043(3)	5.9(1)
C31	−0.6758(6)	−0.1389(6)	−0.7563(2)	6.5(2)
C(32)	−0.6368(6)	−0.2874(8)	−0.8532(3)	7.7(2)
C111	−1.206(1)	−0.032(1)	−0.8345(4)	16.2(7)
C112	−1.041(1)	0.004(1)	−0.7777(5)	14.0(6)
C113	−1.149(1)	−0.1771(8)	−0.7711(4)	11.8(4)
C121	−1.095(1)	−0.3462(7)	−0.8805(5)	13.9(5)
C122	−1.173(1)	−0.1926(9)	−0.9271(6)	16.7(7)
C123	−0.973(1)	−0.263(2)	−0.9465(7)	24(1)
C311	−0.701(1)	−0.229(1)	−0.7175(3)	11.1(4)
C312	−0.538(1)	−0.116(1)	−0.7557(4)	13.9(5)
C313	−0.742(1)	−0.035(1)	−0.7398(4)	18.6(9)
C321	−0.502(1)	−0.258(1)	−0.855(1)	25(1)
C322	−0.656(1)	−0.3971(9)	−0.8264(5)	13.8(5)
C323	−0.680(1)	−0.305(1)	−0.9049(4)	16.4(7)
C400	−0.506(1)	0.043(1)	−0.8748(9)	27(1)
C401	−0.616(1)	0.098(1)	−0.9702(5)	15.2(6)
C402	−0.662(2)	0.230(2)	−0.8842(9)	22.1(9)

stretched Rh–P3 bond (2.399 Å) within the (dtbpm)Rh ring, longer by 0.09 Å than Rh–P1 (2.315 Å). This structural difference in Rh to P bonding manifests itself in widely differing coupling constants ^1J(Rh–P) of only 79 Hz for Rh–P3 and 131 Hz for Rh–P1.

2.5. Spectroscopic observation of alkyne insertions into Rh–Si of 14: model reactions with $MeO_2CC{\equiv}CCO_2Me$

Referring back to Scheme 2, neither the vinyl complex **15** nor its silane adduct **16** could be detected spectroscopically in the stoichiometric or catalytic hydrosilylation reactions. Note, however, that an octahedral Rh^{III} hydrido methyl species similar to the hydrido vinyl system **16** and formed by oxidative addition of $HSi(OEt)_3$ to **13a** must also be an intermediate in the **13a** to **14** transformation. This intermediate could not be detected either, because (as in Thorn and Harlow's complex [44]), methane elimination is too fast. We therefore decided to focus more on the alkyne insertion step into the Rh–Si bond of **14**. For but-2-yne as a substrate, solutions of **14** with an excess of the alkyne gave spectroscopic hints to an insertion equilibrium. We were unable, however, to establish safely the presence of **15** by spectroscopic means. We therefore decided to use the much more electrophilic and reactive alkyne derivative bis(carbomethoxy)acetylene, $MeO_2CC{\equiv}CCO_2Me$. Alkynes have recently been shown by Yamashita et al. [46] to insert into the strong Pt–Si bond of *trans*-$(PEt_3)_2PtX(SiMe_3)$ (X = Br,I) at 90–120°C in a stoichiometric reaction.

When an equivalent of $MeO_2CC{\equiv}CCO_2Me$ is added to a toluene-d_8 solution of **14** at −80°C, in situ NMR spectroscopy (^1H, ^{31}P, ^{13}C) reveals that insertion begins even at this low temperature. At −40°C or above, the reaction is fast and leads to two isomers in a ratio of 3:2, to which we assign the structures **17** and **18** (Scheme 3) with different vinyl stereochemistry.

Our structural assignment is based on the internal consistency of the various NMR data detailed below. We were able to isolate a mixture of both isomers **17** and **18** in analytically pure form as a yellow solid by reacting a solution of (dtbpm)Rh[$Si(OEt)_3$](PMe_3) (**14**) in pentane with a slight excess of bis(carbomethoxy)-

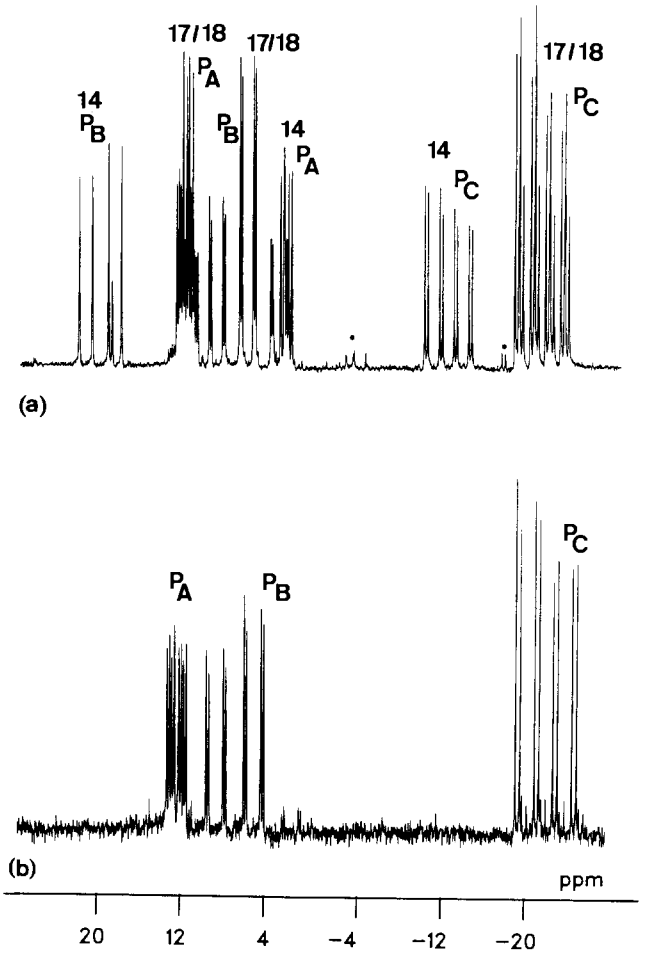

Fig. 7. (a) ^{31}P NMR spectrum of the product mixture obtained in situ (NMR experiment) by reacting **14** with $MeO_2CC{\equiv}CCO_2Me$ at −40°C in toluene-d_8 (molar ratio **14**: alkyne = 1.1:1; therefore complex **14** is still present). (b) ^{31}P NMR spectrum (toluene-d_8, −20°C) of the product mixture **17**/**18** obtained after isolation and recrystallization (ratio of isomers 9:1) (see text and Experimental for details; P_A *trans* to vinyl in **17**/**18** and *trans* to silyl in **14**, P_B *trans* to PMe_3 (= P_C). Asterisks denote impurities.)

acetylene in toluene at −30°C. Crystals could be grown by cooling a saturated solution of **17** and **18** in diethyl ether from −10 to −78°C. Fig. 7(a) displays the ^{31}P NMR spectrum of the product mixture obtained in situ by reacting **14** with $MeO_2CC{\equiv}CCO_2Me$ at −40°C in toluene-d_8 (molar ratio of **14**: alkyne = 1.1 : 1; therefore **14** is still present), and Fig. 7(b) shows the ^{31}P NMR

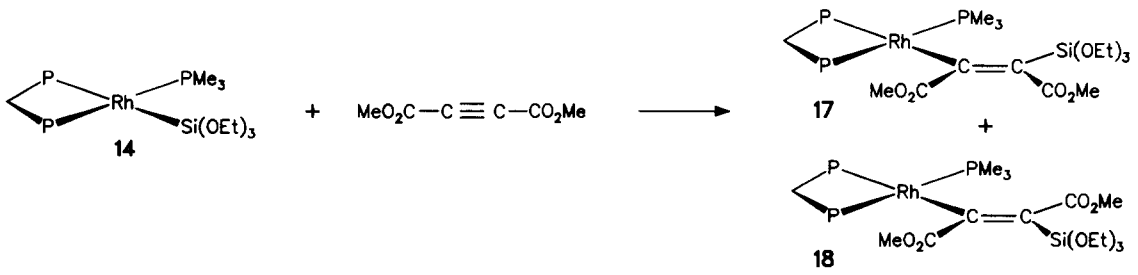

Scheme 3.

spectrum of the product mixture **17/18** obtained after recrystallization (ratio of isomers = 9:1).

There are two very similar sets of ^{31}P signals (ratio 3:2) (Fig. 7(a)), with only a slight chemical shift difference and nearly identical coupling constants. Their multiplicities (ddd) and their characteristic *trans*-P–P coupling constants prove the presence of (dtbpm)Rh-(PMe_3) substructures with intact RhPCP rings and PMe_3 ligands *trans* to one of the P atoms of dtbpm. The Rh–P coupling to the phosphorus *trans* to the substituted vinyl ligand is 97 Hz, 18 Hz larger than the corresponding value in **14**, reflecting the diminished *trans* influence of a vinyl compared with a silyl ligand. The ^1H NMR spectrum displays a pair of singlets for each isomer (3.64, 3.60 and 3.61, 3.44 ppm) for the OCH_3 protons. Compared with the silyl educt **14**, the resonance of the CH_2 hydrogens for the $Si(OEt)_3$ groups appears shifted to higher field at 4.00 ppm. The inequivalence of the two methoxy groups of each isomer is also apparent from $^{13}C\{^1H\}$ NMR: two peaks are found for each product (50.2, 49.6 and 50.6, 49.8 ppm). The OCH_2 carbon atoms of the $Si(OEt)_3$ groups lead to signals at 58.6 and 58.5 ppm, while the triethoxysilyl methyl carbons resonate at 18.9 ppm for both isomers. Four groups of ^{13}C signals are expected for the carbonyl and vinyl carbons of each isomer for the **17/18** mixture: their most reasonable assignment is to the ester carbonyl carbons (broad singlet at 176 and double multiplet at 173 ppm, broad singlet at 177 and double multiplet at 168 ppm) and to the vinyl carbons β to rhodium (multiplets at 131, 127 ppm); for the major isomer the vinyl carbon α to rhodium is detected as a double multiplet at 221 ppm with a characteristic value for *trans*-P–C coupling constants ($^2J(P-C) = 84$ Hz). It is important to mention that we were also able to prepare rhodium compounds, closely related to **17/18**, by insertion of $MeO_2CC{\equiv}CCO_2Me$ and $MeC{\equiv}CMe$ into the Rh–H bond of the hydrido complex (dtbpm)RhH(PMe_3) [48]. The ^{13}C chemical shifts (e.g. of the OCH_3, CO and vinyl carbons) for these vinyl complexes (dtbpm)Rh[$(CO_2Me)C{=}CH(CO_2Me)$](PMe_3) and (dtbpm)Rh[$(Me)C{=}CH(Me)$](PMe_3) are in good agreement with the data found for **17/18**. It is not too surprising that the ^{13}C resonance for the α-vinyl carbon atom of the minor isomer remains undetected. It is a quaternary carbon, additionally spin-coupled to three different P nuclei and a Rh centre, which may well escape detection because of low intensity and signal broadening.

We feel confident, that our spectroscopic data unequivocally establish the structures of **17/18**. These in turn prove the direct insertion of the alkyne $MeO_2CC{\equiv}CCO_2Me$ into the Rh–Si bond of **14**, and we interpret this result as substantial evidence for the correctness of Scheme 3.

We discard alternative structures for **17/18**, in which

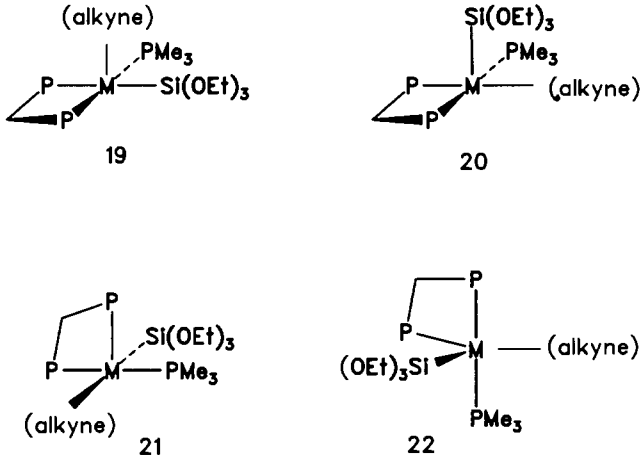

the alkyne has not inserted yet but is only bound to the rhodium centre of **14** through π-coordination. Apart from the expected differences in chemical shifts and coupling constants for such d^8 ML_5 alkyne π-complexes, our spectroscopic data would only allow for pentacoordinate, square-pyramidal (**19**, **20** or **21**) or trigonal bipyramidal (**22**) complexes with an unchanged (dtbpm)Rh(PMe_3) substructure as in **14**, and would require a very improbable rigid (non-rotating) alkyne coordination, because alkyne rotation would make both carbomethoxy groups and both alkyne carbons equivalent in **19–22**. The well known fluxionality of d^8 ML_5 complexes, which would exchange the two P atoms of dtbpm [49], also would have to be absent until ambient temperature. Moreover, the formation and persistence in solution of two structurally very similar isomers cannot be explained reasonably on the basis of alkyne coordination without insertion.

When $HSi(OEt)_3$ is added to a solution of **17/18** at low temperature, hydrosilylation products of $MeO_2C-C{\equiv}CCO_2Me$ analogous to the but-2-yne case in Scheme 2 cannot be isolated. A complex product mixture is obtained which cannot be separated. Apparently this alkyne is ideal for the Rh–Si insertion step but not suited for promoting a clean catalytic hydrosilylation cycle.

A final remark is necessary as to the intermediacy of rhodium hydride complexes and to the possibility of alkyne insertion into Rh–H rather than into Rh–Si bonds. In preliminary NMR experiments we have observed that silyl complex **14** is able to add oxidatively a second molecule of $HSi(OEt)_3$, forming a small amount of the hexacoordinate species (dtbpm)Rh(H)[Si-$(OEt)_3]_2$(PMe_3) in solution, when **14** is treated with an excess of the silane. Reductive elimination of hexakis-(ethoxy)disilane could in principle lead to (dtbpm)Rh-H(PMe_3), the hydride analogue of the methyl complex **13a**, which could open a catalytic hydrosilylation cycle

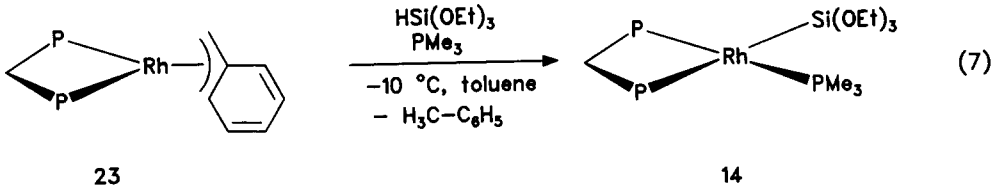

(7)

23 14

via Rh–H insertion, different from Scheme 2. When we react **14** with $HSi(OEt)_3$, however, we do not see any formation of $(EtO)_3SiSi(OEt)_3$, nor do we see any trace of the hydride complex (dtbpm)RhH(PMe_3) which we have recently isolated and characterized independently [48a].

Hence at this point of our investigations, Scheme 2 seems to provide the best mechanistic interpretation for alkyne hydrosilylation by (dtbpm)Rh(alkyl)L complexes.

2.6. Synthesis of (dtbpm)Rh[Si(OEt)$_3$](PMe$_3$) (14) from (dtbpm)Rh(η^3-CH$_2$C$_6$H$_5$) (23)

The silyl complex **14**, accessible from the dimer $[(dtbpm)RhCl]_2$ (**10**) via (dtbpm)RhCl(PMe_3) (**11**) and (dtbpm)RhMe(PMe_3) (**13a**) in three steps, can be prepared more easily if the η^3-benzyl complex (dtbpm)Rh(η^3-$CH_2C_6H_5$) (**23**) is employed as a starting material (Eq. 7).

Compound **23** was prepared in good yield from $[(dtbpm)RhCl]_2$ and two equivalents of (benzyl)MgCl in Et_2O at −10°C, in close analogy to similar complexes $(PR_2(CH_2)_nPR_2)M(\eta^3\text{-}CH_2C_6H_5)$ (M = Rh, Ir; n = 2, 3; R = cyclohexyl, ^{i}Pr) prepared by Fryzuk et al. [50], or to Werner's complexes $(P^iPr_3)_2Rh(\eta^3\text{-}4\text{-}CH_2C_6H_4R)$ (R = H, Me) [51]. Compound **23** is very air-sensitive and decomposes slowly in solution at ambient temperature. It has been characterized by ^{1}H, ^{31}P and ^{13}C NMR spectroscopy; its extreme instability and high reactivity have so far prevented a correct elemental analysis. The fluxional behaviour of $P_2Rh(\eta^3$-benzyl) complexes has been analysed in detail [52] and their chemistry has been explored to some extent. Our complex **23** shows rigid η^3-benzyl coordination at room temperature in solution. The most important advantage of the η^3-benzyl ligand as opposed to, e.g., the simple allyl ligand of the complex (dtbpm)Rh(η^3-C_3H_5) (**24**) [53], which was also synthesized recently, and which is another potential precursor of **14**, lies in its increased lability with respect to η^3/η^1 rearrangements and towards reductive elimination as toluene. For these reasons we anticipated (dtbpm)Rh(η^3-$CH_2C_6H_5$) to be an ideal precursor complex for various oxidative additions, ligand coordination reactions and subsequent transformations at the (dtbpm)Rh fragment in general. The facile synthesis of (dtbpm)Rh[Si(OEt)$_3$](PMe$_3$) from **23** conforms to this concept. The chemistry of (dtbpm)Rh(η^3-$CH_2C_6H_5$) and of its iridium analogue [54] is under intensive investigation in our group.

Certainly more synthetic, structural and mechanistic work is needed to elaborate the catalytic potential of dtbpm containing complexes of rhodium. The present hydrosilylation study has revealed some interesting and novel aspects. Further studies along these lines are under way and will be reported in due course.

3. Experimental

All manipulations were carried out under argon (standard vacuum line, Braun glove-box) and using Schlenk techniques. Solvents were dried according to standard methods, stored under an argon atmosphere and freshly distilled prior to use. $[(dtbpm)RhCl]_2$ (**10**) and (dtbpm)RhCl(PPh_3) were prepared according to published procedures [20]. (dtbpm)Rh(η^3-C_3H_5) was first synthesized (starting from **10** and allylmagnesium bromide) and characterized by Niemeyer [53]. Solutions of methyllithium and benzylmagnesium chloride in diethyl ether and of allylmagnesium chloride in THF were purchased from Aldrich and were degassed and saturated with argon prior to use.

For mass spectrometry, a Finnigan MAT 90 (CI, isobutane, 150 eV) and for IR spectrometry a Nicolet 5 DX instrument were used. Melting points and decom-

Table 9
Preparation of samples for quantitative ^{31}P NMR dissociation equilibrium measurements

No.	Compound (mg)			Solvent C_6D_6 (ml)	Concentration $[E_0]$ (mol l^{-1})
	(dtbpm)RhCl(PPh_3) [20]	PPh_3	**10**		
1	35.5	–		0.767	0.0656
2	35.5	11.9		0.767	0.1249
3	35.5	3.3		0.815	0.0772
4	35.3	5.3		0.777	0.0908
5	34.5	1.8		0.760	0.0734
6	35.7	2.3		0.805	0.0738
7		25.4	46.0	0.829	0.2424
8		16.3	28.0	0.744	0.1686
9		13.3	24.3	0.854	0.1238
10		13.6	25.8	0.835	0.1321

position points were evaluated under an argon atmosphere in a flame-sealed glass tube fixed in a copper block (the values given are uncorrected). Elemental analyses were carried out in the microanalytical laboratory of our institute.

3.1. NMR spectra

A JEOL-FT-JNM-GX 270 instrument was used; ^{1}H (270 MHz, internally referenced to solvent rel. TMS); ^{31}P (109.4 MHz, externally referenced to 85% H_3PO_4); ^{13}C (67.90 MHz, internally referenced to solvent rel. TMS).

For quantitative ^{31}P NMR measurements, the spectra were recorded using a 90° pulse and a relaxation time between the pulses of $5T_1$ (T_1 for (dtbpm)RhCl(PPh_3) at 70°C = 3500 ms). Weighed amounts of **10**, (dtbpm)RhCl(PPh_3), triphenylphosphine and C_6D_6 (Table 9) were placed in an NMR tube with a PTFE valve (glove-box). The spectra were recorded at 70°C.

For equilibrium measurements (^{1}H NMR), in a glove-box 35.5 mg (0.050 mmol) of (dtbpm)RhCl(PPh_3) and 729 mg (0.767 ml) of C_6D_6 ($[E]_0 = 0.065$ mol l^{-1}) were placed in an NMR tube with a PTFE valve. The sample was equilibrated at each temperature (10, 25, 40, 55 and 70°C) for 10 min before taking the spectrum (the temperature was calibrated with a Lambda digital thermometer). Spectra were then obtained sequentially as the sample was heated to the maximum temperature and again as the sample was cooled to the minimum temperature. Thus two points were obtained for each temperature. The relative concentrations were determined by integration of the t-butyl signals of (dtbpm)RhCl(PPh_3) and [(dtbpm)RhCl] and in addition of the CH_2 signals of these compounds.

3.2. Hydrosilylation reactions

A weighed amount of catalyst (typically 5–10 mg) was placed in a Schlenk tube with a PTFE valve, then defined quantities of substrates, but-2-yne and $HSi(OEt)_3$ (1:1) and hex-1-ene and $HSi(OEt)_3$ (1:1), were added. The reactions were monitored by ^{1}H NMR (C_6D_6).

3.3. Crystal structure determination of 10

Data were collected at room temperature on an Enraf-Nonius CAD4 diffractometer with a graphite monochromator. Unit cell dimensions were determined from 25 centred reflections with $23° < \theta < 28°$. Intensities were measured in the θ range 5–55° with Cu Kα radiation. The data were corrected for Lorentz, polarization and crystal decay effects. An empirical absorption correction (DIFABS program [55]) and a correction for extinction [56] were applied. (An absorption correction using ψ scans did not yield better refinement results.) The structure was solved by direct methods (SHELXS-86 [57]); hydrogen atoms were included in calculated positions. Refinement of all non-hydrogen atoms was done by full-matrix least squares using the structure determination package SDP [58]. The difference electron density maps indicate that at least nine of the 16 t-butyl groups are disordered. Attempts to resolve these disorders failed. The two independent molecules in the crystal are connected by a local, non-crystallographic 2_1 axis parallel to a. The orientations of all eight molecules in the unit cell are different. There is no close similarity to a higher symmetric space group. Further details of the structure determination are available on request from the Fachinformationszentrum Karlsruhe, Gesellschaft für wissenschaftlich-technische Information mbH, D-76344 Eggenstein-Leopoldshafen, Germany, quoting the depository number CSD-58222.

3.4. Crystal structure determination of 14

Compound **14** crystallizes as orange–red blocks. A single crystal with the approximate dimensions 0.2 × 0.25 × 0.5 mm was chosen for the X-ray investigations, which were performed on an (Enraf-Nonius) CAD4 diffractometer with Mo Kα radiation and a graphite monochromator at 202 K. The lattice parameters were determined with 100 precisely centred high-angle reflections. For the structure determination 7876 intensities (Friedel pairs) measured with an ω-scan from $\theta = 3–27°$ were used. Intensity data were corrected for Lorentz and polarization effects [59] and absorption. The positions of the Rh and P atoms were deduced from a Patterson synthesis [60]. Subsequent difference Fourier synthesis revealed the positions of the Si, O and C atoms. Hydrogen atoms were calculated in idealized positions [61]. The final full-matrix refinement with anisotropic displacement parameters led to R values $R_1 = 0.047$ and $wR_2 = 0.132$ [61]. Crystallographic details are given in Table 6, selected bond distances and angles in Table 7 and positional and equivalent isotropic displacement parameters in Table 8. Further details have been deposited at the Fachinformationszentrum Karlsruhe (see above) as Supplementary Material with depository number CSD-58383.

3.5. Synthesis of (dtbpm)RhMe(PMe_3), 13a

To a suspension of 208 mg (0.402 mmol) of (dtbpm)RhCl(PMe_3) in pentane (20 ml), 0.39 ml of a 1.35 m (0.523 mmol) solution of methyllithium in diethyl ether were added at 0°C. The reaction mixture was stirred for 12 h while slowly warming to room temperature. The solvent was removed under vacuum and the product extracted with pentane. The orange

solution was filtered through a plug of Celite, concentrated until the beginning of crystallization and cooled to −30°C to yield 150 mg (75%) of orange crystalline **13a**, m.p. 105–108°C Anal. Calc. for $C_{21}H_{50}P_3Rh$ (498.2) C 50.60; H 10.11; P 18.64; Found: C 50.39; H 10.03; P 19.30%. ^{1}H NMR (C_6D_6): 0.42 ppm (m, 3H, Rh–CH_3); 1.25 (dm, ^2J(P–H) = 6.0 Hz, 9H, $P(CH_3)_3$); 1.30 (d, ^3J(P–H) = 11.1 Hz, 18H, P^{t}Bu$_2$); 1.41 (d, ^3J(P–H) = 11.5 Hz, 18H, P^{t}Bu$_2$); 3.00 ("t", 2H, PCH_2P). ^{31}P NMR (C_6D_6): −13.0 ppm (ddd, ^1J(Rh–P) = 153 Hz, ^2J(P–P) = 367 Hz, ^2J(P–P) = 31.1 Hz, PMe_3); 13.4 (ddd, ^1J(Rh–P) = 140 Hz, ^2J(P–P) = 367 Hz, ^2J(P–P) = 15.5 Hz, P *trans* PMe_3); 21.4 (ddd, ^1J(Rh–P) = 96.0 Hz, ^2J(P–P) = 31.1 Hz, ^2J(P–P) = 15.5 Hz, P *trans* CH_3). ^{13}C NMR (C_6D_6): −9.6 ppm (dm, ^2J(P–C) = 72.8 Hz, Rh-CH_3); 19.0 (dm, ^1J(P–C) = 19.3 Hz, $P(CH_3)_3$); 31.4 ("t", $C(CH_3)_3$); 33.8 ("t", $C(CH_3)_3$); 35.3 (m, $C(CH_3)_3$); 36.6 (m, PCH_2P). IR (KBr); ν (cm^{-1}) = 2898 (s, br.), 1479 (s), 1386 (m), 1363 (s), 1292 (w), 1272 (m), 1174 (s), 1082 (m), 1018 (w), 944 (s), 843 (w), 809 (m), 716 (m), 682 (m), 664 (s), 580 (w), 561 (w), 507 (w), 479 (m), 417 (w). MS (CI): m/z(%) = 498 (100) [M^+]: correct isotope pattern; 483 (82) [$M^+ - CH_3$], 441 (20) [$M^+ - C_4H_9$], 426 (10) [$M^+ - CH_3 - C_4H_9$], 422 (1) [$M^+ - PMe_3$], 407 (2) [$M^+ - CH_3 - PMe_3$], 369 (2) [$M^+ - CH_3 - 2C_4H_9$], 365 (3) [$M^+ - PMe_3 - C_4H_9$], 351 (2) [$M^+ - CH_3 - C_4H_9 - PMe_3$], 305 (8) [dtbpm$^+$], 248 (17) [dtbpm$^+ - C_4H_9$], 191 (4) [dtbpm$^+ - 2C_4H_9$].

3.6. Synthesis of (dtbpm)Rh[Si(OEt$_3$)](PMe$_3$), 14

(a) A 226 mg (0.454 mmol) amount of (dtbpm)Rh-Me(PMe_3) (**13a**) was dissolved in 9 ml of pentane in a Schlenk tube. At −10°C 117 μl (0.634 mmol) of $HSi(OEt)_3$ were added. The colour of the solution immediately turned from orange to red. After stirring at −10°C for 3 h, the solvent was reduced in volume under vacuum until the beginning of crystallization, still at a temperature of −10°C. On cooling to −30°C the main portion of the product crystallized. The remaining solution was filtered off via a cannula. The product was dried at 0°C in vacuum.

(b) A 132 mg (0.264 mmol) amount of Rh(dtbpm)-(η^3-$CH_2C_6H_5$) (**23**) was dissolved in toluene (3 ml) in a Schlenk tube. At −10°C 0.29 ml of a 1 m solution of trimethylphosphine in toluene and 53 μl (0.287 mmol) of $HSi(OEt)_3$ were added. The red solution was stirred at −10°C for 5 h. The solvent was removed under vacuum and the residue was dissolved in pentane (1 ml, −10°C). Crystallization at −30°C yielded **14** (80–90%) as red crystals. Anal. Calc. for $C_{26}H_{62}O_3P_3RhSi$ (646.7) C 48.29; H 9.66; Rh 15.91; Found: C 47.51; H 9.65; Rh 16.43% ^{1}H NMR (toluene-d_8, 0°C): 4.15 ppm (q, ^3J(H–H) = 6.8 Hz, 6H, $Si(OCH_2CH_3)_3$); 3.18 ("t", 2H, PCH_2P); 1.50 (d, ^3J(P–H) = 12.7 Hz, 18H, P^{t}Bu$_2$ and dm, 9H, $P(CH_3)_3$); 1.41 (t, ^3J(H–H) = 7.3 Hz, 9H, $Si(OCH_2CH_3)_3$); 1.23 (d, ^3J(P–H) = 11.7 Hz, 18H, P^{t}Bu$_2$). ^{31}P NMR (toluene-d_8, 0°C): 21.9 ppm (dd, ^1J(Rh–P) = 132 Hz, ^2J(P–P) = 293 Hz, *cis*-coupling of ring-P atoms not resolved, P *trans* PMe_3); 4.9 (dd + sat, ^1J(Rh–P) = 79.1 Hz, ^2J(P–P) = 32.5 Hz, ^2J(Si–P) = 209 Hz, *cis*-coupling of ring-P atoms not resolved, P *trans* Si); 12.5 (ddd + sat, ^1J(Rh–P) = 150 Hz, ^2J(P–P) = 293 Hz, ^2J(P–P) = 31.1 Hz, PMe_3). ^{13}C NMR (C_6D_6, 10°C): 56.8 ppm (s, $Si(OCH_2CH_3)_3$); 36.5 (m, PCH_2P); 35.8 (m, $C(CH_3)_3$); 34.9 (m, $C(CH_3)_3$); 31.4 (d, ^2J(P–C) = 6.7 Hz, $C(CH_3)_3$); 31.2 (d, ^2J(P–C) = 7.7 Hz, $C(CH_3)_3$); 23.2 (dm, ^1J(P–C) = 24.0 Hz, $P(CH_3)_3$); 19.3 (s, $Si(OCH_2CH_3)_3$).

3.7. Reaction of (dtbpm)Rh[Si(OEt)$_3$](PMe$_3$), 14, with bis(carbomethoxy)acetylene (MeO$_2$OC≡CCO$_2$Me) to 17 and 18

(a) In situ NMR experiment

A 38.4 mg (0.059 mmol) amount of **14** was placed in an NMR tube and dissolved in 0.6 ml of toluene-d_8 at −60°C, then 6.7 μl (0.055 mmol) of bis(carbomethoxy)-acetylene were added. After the solution had been degassed once, the tube was flame sealed and kept at −78°C until NMR measurements. ^{1}H NMR (toluene-d_8, −40°C, see Fig. 7(a); complex **14** still present): 4.00 ppm (q, ^3J(H–H) = 6.3 Hz, 6H, $Si(OCH_2CH_3)_3$); 3.64, 3.61, 3.60 and 3.44 (s, 3H, CO_2CH_3); 2.81 ("t", 2H, PCH_2P), 1.50–1.10 (54H, P^{t}Bu$_2$, $P(CH_3)_3$, $Si(OCH_2CH_3)_3$). ^{31}P-NMR (toluene-d_8, −40°C): major isomer: 13.2 ppm (ddd, ^1J(Rh–P) = 94.0 Hz, ^2J(P–P) = 20.0 Hz, ^2J(P–P) = 35.7 Hz, P *trans* vinyl); 8.9 (ddd, ^1J(Rh–P) = 135 Hz, ^2J(P–P) = 305 Hz, ^2J(P–P) = 20.0 Hz, P *trans* PMe_3); −20.2 (ddd, ^1J(Rh–P) = 155 Hz, ^2J(P–P) = 305 Hz, ^2J(P–P) = 37.0 Hz, PMe_3); minor isomer: 12.2 ppm (overlapped by signal of major isomer); 7.3 (ddd, ^1J(Rh–P) = 138 Hz, ^2J(P–P) = 309 Hz, ^2J(P–P) = 17.1 Hz, P *trans* PMe_3); −21.3 (ddd, ^1J(Rh–P) = 155 Hz, ^2J(P–P) = 309 Hz, ^2J(P–P) = 37.0 Hz, PMe_3). ^{13}C NMR (toluene-d_8, −10°C): major isomer: 30.7, 30.9, 31.7 and 32.0 ppm (d, ^2J(P–C) = 6.6 Hz, $C(CH_3)_3$); minor isomer: 30.7, 30.9, 31.9 and 32.1 ppm (d, ^2J(P–C) = 6.0 Hz, $C(CH_3)_3$); $C(CH_3)_3$ as multipletts at 34.0–35.2 and 36.6 ppm; 37.1 ppm (m, PCH_2P); 18.9 ppm (s, $Si(OCH_2CH_3)_3$); major isomer: 49.6 and 50.2 ppm (s, OCH_3); 58.6 ppm (s, $Si(OCH_2CH_3)_3$); 176 ppm (br. s, CO_2Me), 173 ppm (dm, CO_2Me); minor isomer: 49.8 and 50.6 ppm (s, OCH_3); 58.5 ppm (s, $Si(OCH_2CH_3)_3$); 177 ppm (br. s, CO_2Me), 168 ppm (dm, CO_2Me); overlapped by signals of solvent: $P(CH_3)_3$ 20.1 and 20.3 ppm. ^{13}C NMR ($CD_3C_6D_{11}$, 0°C): major isomer: 221 ppm (dm, ^2J(P–C) = 84.0 Hz, C-1 vinyl); 131 ppm (m, C-2 vinyl); 20.5 ppm (dm, ^1J(P–C) = 21.0 Hz, $P(CH_3)_3$); minor isomer: 127 ppm (m, C-2 vinyl); 20.7 ppm (dm, ^1J(P–C) = 22.0 Hz, $P(CH_3)_3$).

(b) Isolation of 17 / 18 product mixture

A 300 mg (0.464 mmol) amount of (dtbpm)Rh[Si(OEt)$_3$](PMe$_3$) (**14**) was dissolved in 5 ml of pentane at −30°C, then a solution of 60 μl (0.488 mmol) of bis(carbomethoxy)acetylene in 1 ml of toluene was added. After stirring at −30°C for 2 h, the solvent was removed in vacuo and the yellow residue was washed with pentane at −30°C and dried in vacuum. ^{1}H and ^{31}P NMR spectra (toluene-d$_8$, −20°C): see (a) (only signals for **17/18** are present). Crystals could be grown by cooling a saturated solution of **17/18** in diethyl ether from −10 to −78°C. ^{1}H and ^{31}P NMR spectra (toluene-d$_8$, −20°C): see (a) (ratio of isomers 9:1; see also Fig. 7(b)).

3.8. Synthesis of (dtbpm)Rh(η^3-CH$_2$C$_6$H$_5$), 23

To 400 mg (0.450 mmol) of [Rh(dtbpm)Cl]$_2$ (**10**), 5 ml THF were added. At a temperature of −10°C, 1 ml of a 1 m solution of C$_6$H$_5$CH$_2$MgCl in diethyl ether was added. The suspension was stirred at −10°C for 24 h. During the reaction the colour turned red and a precipitate was formed. The solvent was removed under vacuum and the product was extracted with pentane. The orange pentane solution was filtered through a plug of Celite, concentrated until the beginning of crystallization and cooled to −30°C to yield 329 mg (72%) of **23**. The product can be recrystallized from THF at −30°C. ^{1}H NMR (C$_6$D$_6$): 1.14 ppm (d, ^3J(P–H) = 12.2 Hz, 18H, P^{t}Bu$_2$); 1.28 (d, ^3J(P–H) = 12.7 Hz, 18H, P^{t}Bu$_2$); 2.34 (d, J = 6.35 Hz, 2H, CH_2C$_6$H$_5$); 3.04 ("t", 2H, PCH$_2$P); 5.89 (d, J = 7.3 Hz, 2 H, *o*-H (phenyl)); 6.61 (t, 1 H, *p*-H (phenyl)); 7.33 (t, J = 7.3 Hz, 2 H, *m*-H (phenyl)). ^{31}P NMR (C$_6$D$_6$): 29.2 ppm (dd, ^2J(P–P) = 28.5 Hz, ^1J(Rh–P) = 151 Hz); 41.5 (dd, ^2J(P–P) = 28.5 Hz, ^1J(Rh–P) = 230 Hz). ^{13}C NMR (C$_6$D$_6$): 28.8 ppm (dd, J = 9.3 Hz, J = 37.5 Hz, CH_2C$_6$H$_5$); 31.5 (d, ^2J(P–C) = 7.8 Hz, C(CH_3)$_3$); 35.2 (m, C(CH$_3$)$_3$); 35.5 (m, C(CH$_3$)$_3$); 39.7 (m, PCH$_2$P); 105.6 (dd, J = 9.4 Hz, J = 1.1 Hz, *o*-C (phenyl)); 117.9 (m, *p*-C (phenyl)); 118.6 (m, *ipso*-C(phenyl)); 132.7 (m, *m*-C (phenyl)).

3.9. Synthesis of (dtbpm)Rh(η^3-C$_3$H$_5$), 24

A 0.490 g (0.554 mmol) amount of [Rh(dtbpm)Cl]$_2$ (**10**) was dissolved in 50 ml of THF and 0.67 ml of a 2 m solution of allylmagnesiumchloride in THF were added at 0°C. The reaction mixture was stirred for 12 h, during which time it warmed to room temperature. The solvent was removed under vacuum and the product extracted with pentane. The yellow solution was filtered through a plug of Celite, concentrated under vacuum and cooled to −30°C to yield 186 mg (75%) of yellow needles, m.p. (decomp.) 187°C. Anal. Calc. for C$_{20}$H$_{43}$P$_2$Rh (448.1): C 53.57; H 9.60; Found: C 53.49; H 9.57%. ^{1}H NMR (C$_6$D$_6$): 1.22 ppm (d, ^3J(P–H) = 12.2 Hz, 18H, P^{t}Bu$_2$); 1.31 (d, ^3J(P–H) = 12.2 Hz, 18H, P^{t}Bu$_2$); 2.18 (dd, ^3J(P–H) = 13.2 Hz, ^3J(H–H) = 6.8 Hz, 2H, allyl-H (*anti*)); 3.21 (d of t, ^2J(H–H) = 16.1 Hz, ^2J(P–H) = 7.3 Hz, 1H, PCHHP); 3.33 (d of t of d, ^2J(H–H) = 16.1 Hz, ^2J(P–H) = 7.3 Hz, ^3J(Rh–H) = 1.0 Hz, 1H, PCHHP); 3.85 (d, ^3J(H–H) = 6.8 Hz, 2H, allyl-H (*syn*)); 4.75 (m, ^3J(H–H) = 7 Hz, ^2J(Rh–H) = 2 Hz, 1H, CH$_2$CHCH$_2$). ^{31}P NMR (C$_6$D$_6$): 35.6 ppm (d, ^1J(Rh–P) = 174 Hz). ^{13}C NMR (C$_6$D$_6$): 31.3 ppm (t of d, J = 3.6 Hz, J = 1.0 Hz, C(CH_3)$_3$); 31.6 (t, J = 3.6 Hz, C(CH_3)$_3$); 34.9–35.1 (m, C(CH$_3$)$_3$); 40.1 (m, PCH$_2$P); 47.0 (dec, C(terminal)); 106 (d of t, ^1J(Rh–C) = 5.5 Hz, J(P–C) = 1.9 Hz, C(central)). IR (KBr): ν (cm^{-1}) = 3033 (m), 2987–2892 (s, br), 2362 (w), 1915 (w), 1699 (w), 1636 (w), 1480 (s), 1459 (m), 1388 (m), 1363 (s), 1261 (w), 1177 (s), 1087 (m), 1017 (m), 997 (m), 960 (w), 932 (w), 849 (m), 811 (s), 735 (w), 714 (w), 674 (m), 589 (w), 565 (w), 514 (w), 485 (m), 452 (m). MS (Cl) *m/z* (%): 448 (100) [M$^+$]: correct isotope pattern; 407 (3) [M$^+$ − C$_3$H$_5$], 391 (5) [M$^+$ − C$_4$H$_9$].

Acknowledgements

We are grateful to the Deutsche Forschungsgemeinschaft, the Fonds der Chemischen Industrie, BASF, Degussa, Wacker-Chemie and Hewlett-Packard for their support of this work. We also thank Professors G.E. Herberich, RWTH Aachen, and H. Schmidbaur, TU Munich, for providing X-ray facilities and H.-H. Niemeyer for his experimental contributions to the synthesis of (dtbpm)Rh(η^3-C$_3$H$_5$) in the early stages of these studies. We appreciate the assistance of Dr. U. Englert with the X-ray structure of **10**.

References and notes

[1] (a) J.F. Harrod and A.J. Chalk, in I. Wender and P. Pino (eds.), *Organic Synthesis via Metal Carbonyls*, Vol. 2, Wiley, New York, 1977, p. 673; (b) J.L. Speier, *Homogeneous Catalysis of Hydrosilation by Transition Metals: Advances in Organometallic Chemistry*, Vol. 17, Academic Press, New York, 1979, p. 673.

[2] (a) L.N. Lewis, *J. Am. Chem. Soc.*, *112* (1990) 5998; (b) L.N. Lewis, R.J. Uriarte and N. Lewis, *J. Catal.*, *127* (1991) 67.

[3] T.D. Tilley and I. Ojima, in S. Patai and Z. Rappoport (eds.), *The Chemistry of Organic Silicon Compounds*, Wiley, New York, 1989, Chapters 24 and 25.

[4] A.J. Chalk and J.F. Harrod, *J. Am. Chem. Soc.*, *87* (1965) 16.

[5] T.A. Albright, J.K. Burdett and M.H. Whangbo, *Orbital Interactions in Chemistry*, Wiley, New York, 1985.

[6] H.H. Karsch, *Z. Naturforsch., Teil B.*, *38* (1983) 1027.

[7] (a) K. Jonas, personal communication; (b) J.S. Yu and I.P. Rothwell, *J. Chem. Soc., Chem. Commun.*, (1992) 632; (c) F.I. Joslin, J.T. Mague and D.M. Roundhill, *Polyhedron*, *10* (1991) 1713.

[8] (a) P. Hofmann, H. Heiss, P. Neiteler, G. Müller and J. Lach-

mann, *Angew. Chem.*, *102* (1990) 935; *Angew. Chem., Int. Ed. Engl.*, *29* (1990) 880; (b) P. Hofmann, in N. Auner and J. Weis (eds.), *Organosilicon Chemistry*, VCH, Weinheim, 1994, p. 231.

[9] (a) P. Hofmann and G. Unfried, *Chem. Ber.*, *125* (1992) 659; (b) P. Hofmann and T. Gerl, Paper presented at the 207th ACS National Meeting, San Diego, March 13–17, 1994 (Abstract 513).

[10] P. Hofmann, L.A. Perez-Moya, O. Steigelmann and J. Riede, *Organometallics*, *11* (1992) 1167.

[11] P. Hofmann, L.A. Perez-Moya, M.E. Krause, O. Kumberger and G. Müller, *Z. Naturforsch., Teil B*, *45* (1990) 897.

[12] P. Hofmann, M.E. Krause and G. Unfried, unpublished results.

[13] (a) P. Hofmann, H. Heiss and G. Müller, *Z. Naturforsch., Teil B.*, *42* (1987) 395; (b) P. Hofmann, in A. de Meijere and H. tom Dieck (eds.), *Organometallics in Organic Synthesis*, Springer, Berlin, 1987.

[14] (a) A.J. Kunin and R. Eisenberg, *Organometallics*, *7* (1988) 2124; *J. Am. Chem. Soc.*, *108* (1986) 535; (b) W.D. Jones and E.T. Hessell, *Organometallics*, *9* (1990) 718; (c) M. Tanaka, T. Sakakura, Y. Tokonuga and T. Sodeyama, *Chem. Lett.*, (1987) 2373; (d) J.A. Maguire, W.T. Boese and A.S. Goldman, *J. Am. Chem. Soc.*, *111* (1989) 7088; *Coord. Chem. Rev.*, *97* (1990) 179; K. Nomura and Y. Saito, *J. Chem. Soc., Chem. Commun.*, (1988) 161; *J. Mol. Catal.*, *54* (1989) 57. (e) T. Fujii and Y. Saito, *J. Chem. Soc., Chem. Commun.*, (1990) 757; J.A. Maguire and A.S. Goldman, *J. Am. Chem. Soc.*, *113* (1991) 6706; (f) A.L. Casalnuovo, J.C. Calabrese and D. Milstein, *J. Am. Chem. Soc.*, *110* (1988) 6738; (g) A.A. Zlota, F. Frolow and D. Milstein, *J. Chem. Soc., Chem. Commun.*, (1989) 1826; (h) W.T. Boese and A.S. Goldman, *Organometallics*, *10* (1991) 782; (i) J.P. Kovalev, K.V. Yevdakov, Yu.A. Strelenko, M.G. Vinogradov and G.I. Nikishin, *J. Organomet. Chem.*, *386* (1990) 139; (j) M.J. Burk and R.H. Crabtree, *J. Am. Chem. Soc.*, *109* (1987) 8025.

[15] (a) J.A. Osborn, F.H. Jardine, J.F. Young and G. Wilkinson, *J. Chem. Soc. A.*, (1966) 1711; (b) J.P. Collman, L.S. Hegedus, R.J. Norton and R.G. Finke, *Principles and Applications of Organotransition Metal Chemistry*, University Science Books, Mill Valley, CA, 1987; (c) J. Halpern, T. Okamoto and A. Zakhariev, *J. Mol. Catal.*, *2* (1976) 65.

[16] (a) T. Sakakura, T. Sodeyama, K. Sasaki, K. Wada and M. Tanaka, *J. Am. Chem. Soc.*, *112* (1990) 7221; T. Sakakura, T. Sodeyama and M. Tanaka, *New. J. Chem.*, *13* (1989) 737, and references cited therein; (b) P.C. Ford, T.L. Netzel, C.T. Spillett and D.B. Pourreau, *Pure Appl. Chem.*, *62* (1990) 1091; C.T. Spillett and P.C. Ford, *J. Am. Chem. Soc.*, *111* (1989) 1932.

[17] (a)D. Seyferth, A.G. Davies, E.O. Fischer, J.F. Normant and O.A. Reutov (eds.), *Organometallic Chemistry Review, Journal of Organometallic Chemistry Library*, Vol. 5, Elsevier, Amsterdam, 1977; (b) E. Lukevics and M.G. Voronkov, *Organic Insertion Reactions of Group IV Elements*, Consultants Bureau, New York, 1966; (c) I. Ojima, M. Kumagai and Y. Nagai, *J. Organomet. Chem.*, *66* (1974) C14; (d) H.M. Dickers, R.N. Haszeldine, A.P. Mather and R.V. Parish, *J. Organomet. Chem.*, *161* (1978) 91; (e) K.A. Brady and T.A. Nile, *J. Organomet. Chem.*, *206* (1981) 299; (f) H. Watanabe, T. Kitahara, T. Motegi and Y. Nagai, *J. Organomet. Chem.*, *139* (1977) 215; B. Marciniec, W. Duczmal, W. Urbaniak and E. Sliwinska, *J. Organomet. Chem.*, *285* (1990) 319.

[18] (a) C. Meier, Diplomarbeit, Technische Universität München, 1989; (b) A. Dedieu, *Inorg. Chem.*, *19* (1980) 375.

[19] (a) J.M. Brown and A.R. Lucy, *J. Chem. Soc., Chem. Commun.* (1984) 914; (b) J.M. Brown, P.L. Evans and A.R. Lucy, *J. Chem. Soc., Perkin Trans. 2* (1987) 1589.

[20] P. Hofmann, C. Meier, U. Englert and M.U. Schmidt, *Chem. Ber.*, *125* (1992) 353.

[21] (a) E.P. Wasserman, R.G. Bergman and C.B. Moore, *J. Am. Chem. Soc.*, *110* (1988) 6076; (b) B.H. Weiller, E.P. Wasserman, C.B. Moore and R.G. Bergman, *J. Am. Chem. Soc.*, *115* (1993) 4326; (c) R.G. Bergman, *J. Organomet. Chem.*, *400* (1990) 273; (d) B.H. Weiller, E.P. Wasserman, R.G. Bergman, C.B. Moore and G.C. Pimentel, *J. Am. Chem. Soc.*, *111* (1989) 8288; (e) M.B. Sponsler, B.M. Weiller, P.O. Stoutland and R.G. Bergman, *J. Am. Chem. Soc.*, *111* (1989) 6841.

[22] (a) D.M.-T. Chan, T.B. Marder, D. Milstein and N.J. Tayler, *J. Am. Chem. Soc.*, *109* (1987) 6385; (b) T.B. Marder, D.M.-T. Chan, W.C. Fultz, J.C. Calabrese and D. Milstein, *J. Chem. Soc., Chem. Commun.*, (1987) 1885.

[23] Data are available for about 35 X-ray structure determinations of η^2-dtbpm complexes.

[24] L.F. Dahl, C. Martell and D.L. Wampler, *J. Am. Chem. Soc.*, *83* (1961) 1761.

[25] K.A. Klanderman, *Diss. Abstr.*, *25* (1965) 6253; (see also Ref. [11] in [30]).

[26] J.J. Bonnet, Y. Jeannin, P. Kalck, A. Maisonnat and R. Poilblanc, *Inorg. Chem.*, *14* (1975) 743.

[27] R.C. Schnabel and D.M. Roddick, *Inorg. Chem.*, *32* (1993) 1513.

[28] J.A. Ibers and R.G. Snyder, *Acta Crystallogr.*, *15* (1962) 923.

[29] M.D. Curtis, W.M. Butler and J. Greene, *Inorg. Chem.*, *17* (1978) 2928.

[30] P. Binger, J. Haas, G. Glaser, R. Goddard and C. Krüger, *Chem. Ber.*, *127* (1994) 1927.

[31] B.D. Murray, H. Hope, J. Hvoslef and P.P. Power, *Organometallics*, *3* (1984) 657.

[32] R.H. Summerville and R. Hoffmann, *J. Am. Chem. Soc.*, *98* (1976) 7240.

[33] Substitution of ^{t}Bu groups (dhpm vs. dtbpm) in our MO calculations does not affect the electronic structure of these molecules.

[34] Program SCHAKAL 88, Egbert Keller, Universität Freiburg.

[35] (a) P.B. Hitchcock, M. McPartlin and R. Mason, *J. Chem. Soc., Chem. Commun.* (1969) 1367; M.J. Bennett and P.B. Donaldson, *Inorg. Chem.*, *16* (1977) 655; (b) R.A. Jones, F.M. Real, G. Wilkinson, A.M.R. Galas and M.B. Hursthouse, *J. Chem. Soc., Dalton Trans.*, (1981) 126; (c) R.A. Jones, F.M. Real, G. Wilkinson, A.M.R. Galas, M.B. Hursthouse and K.M.A. Malik, *J. Chem. Soc., Dalton Trans.* (1980) 511; (d) M.A. Bennett, G.B. Robertson, T.W. Turney and P.O. Whimp, *J. Chem. Soc., Chem. Commun.*, (1971) 762.

[36] (a) J. Wolf, L. Brandt, A. Fries and H. Werner, *Angew. Chem., 102* (1990) 584; *Angew. Chem., Int. Ed. Engl., 29* (1990) 510; (b) D. Schneider and H. Werner, *Angew. Chem., 103* (1991) 710; *Angew. Chem., Int. Ed. Engl., 30* (1991) 700.

[37] N.A. Donskaya, N.M. Yur'eva and I.P. Beletskaya, *Mendeleev Commun.*, (1992) 136.

[38] J. Halpern and C.S. Wong, *J. Chem. Soc., Chem. Commun.*, (1973) 629.

[39] D.A. Wink and P.C. Ford, *J. Am. Chem. Soc., 109* (1987) 436.

[40] D.E. Budd, D.G. Holah, A.N. Hughes and B.C. Hui, *Can. J. Chem., 52* (1974) 775.

[41] (a) K.W. Chiu, H.S. Rzepa, R.N. Sheppard, G. Wilkinson and W.-K. Wong, *Polyhedron, 1* (1982) 809; (b) K.W. Chiu, H.S. Rzepa, R.N. Sheppard, G. Wilkinson and W.-K. Wong, *J. Chem. Soc., Chem. Commun.*, (1982) 482.

[42] A.A. Gonzalez, K. Zhang, S.P. Nolan, R.L. de la Vega, S.L. Mukerjee and C.D. Hoff, *Organometallics, 7* (1988) 2429.

[43] The X-ray structure determination of the neopentyl complexes (dtbpm)RhNp(CO) **13c** and its iridium analogue (dtbpm)IrNp(CO) were carried out by J. Riede, P. Bissinger and U. Thewalt, respectively; P. Hofmann, C. Meier and A. Maier, unpublished results.

[44] D.L. Thorn and R.L. Harlow, *Inorg. Chem., 29* (1990) 2017.

[45] M. Aizenberg and D. Milstein, *Angew. Chem., 106* (1994) 344; *Angew. Chem., Int. Ed. Engl., 33* (1994) 317; see also U. Schubert, *Angew. Chem., 106* (1994) 435; *Angew. Chem., Int. Ed. Engl., 33* (1994) 419.

[46] H. Yamashita, M. Tanaka and M. Goto, *Organometallics, 12* (1993) 988.

[47] (a) H. Sakurai, Y. Kamiyama and Y. Nakadaira, *J. Am. Chem. Soc., 97* (1975) 931; (b) Y. Tsuji and Y. Obora, *J. Am. Chem. Soc., 113* (1991) 9368; (c) T. Hayashi, T.-A. Kobayashi, A.M. Kawamoto, H. Yamashita and M. Tanaka, *Organometallics, 9* (1990) 280. Note added in proof: catalytic alkyne hydrosilylation by insertion into Ru–Si bonds has been observed by Roper (reported at the Int. Symp. on Molecular Reaction Mechanisms Involving Transition Metals, Florence, October 25–30, 1994, Abstract Vol., p. 8, manuscript in preparation).

[48] (a) The hydride complex (dtbpm)RhH(PMe_3) was synthesized by reacting (dtbpm)RhMe(PMe_3) with H_2 (1 bar) at 0°C and was fully characterized: C. Meier, Dissertation, Technische Universität München, 1992. (b) The rhodium vinyl complexes (dtbpm)Rh(vinyl)(PMe_3) (vinyl ligand=$(CO_2Me)C{=}CH(CO_2Me)$ and (Me)C=CH(Me)) were synthesized by reacting (dtbpm)RhH(PMe_3) with bis(carbomethoxy)acetylene and but-2-yne, respectively (in each case only one isomer is formed). The complexes were characterized by ^1H, ^{31}P and ^{13}C NMR spectroscopy and IR and mass spectrometry and elemental analysis. Synthetic details will be published separately [48c]. ^{13}C NMR (C_6D_6, room temperature) (dtbpm)Rh[$(CO_2Me)C{=}CH(CO_2Me)$](PMe_3): 205 ppm (dm, ^2J(P–C) = 88 Hz, C–1 vinyl); 177 (m, Rh[C=CH(CO_2Me)]); 162 (dm, Rh[(MeO_2C)C=C]); 119 ("t", J = 4.9 Hz, C-2 vinyl); 50.0 and 49.9 (s, CO_2CH_3); 37.2, 35.8, 35.2, 34.0 (m, $PC(CH_3)_3$); 35.0 ("t", PCH_2P); 31.3 (br. d, $PC(CH_3)_3$); 20.0 (dm, ^1J(P–C) = 22 Hz, $P(CH_3)_3$). ^{13}C NMR (C_6D_6, room temperature) (dtbpm)Rh[(Me)C=CH(Me)](PMe_3): 164 ppm (dddd, ^2J(P–C) = 83 Hz, ^1J(Rh–C) = 28 Hz, ^2J(P–C) = 12 Hz, ^2J(P–C) = 17 Hz, C-1 vinyl); 120 (m, C-2 vinyl); 36.2 ("t", PCH_2P); 34.3, 35.6, 35.9 (m, $PC(CH_3)_3$); 31.9, 31.4 (br, s, $PC(CH_3)_3$); 24.3 (m, Rh[C=CH(CH_3)]); 19.7 (dm, ^1J(P–C) = 20.4 Hz, $P(CH_3)_3$); 14.8 (dm, J = 7.7 Hz, Rh[(CH_3)C=C]). (c) P. Hofmann and C. Meier, in preparation.

[49] The pentacoordinate iridium complex (dtbpm)$IrH(CO)_2$ is fluxional at room temperature, exchanging the P atoms of the dtbpm ligand; A. Maier, Dissertation, Technische Universität München, 1992.

[50] M.D. Fryzuk, D.H. McConville and S.J. Rettig, *J. Organomet. Chem., 445* (1993) 245.

[51] M. Schäfer, N. Mahr, J. Wolf and H. Werner, *Angew. Chem., 105* (1993) 1377; *Angew. Chem., Int. Ed. Engl., 32* (1993) 1315.

[52] H. Werner, M. Schäfer, O. Nürnberger and J. Wolf, *Chem. Ber., 127* (1994) 27.

[53] H.-H. Niemeyer, Diplomarbeit, Technische Universität München, 1992.

[54] P. Hofmann and O. Steck, unpublished results.

[55] N. Walker and D. Stuart, *Acta Crystallogr., Sect. A, 39* (1983) 158.

[56] W.H. Zachariasen, *Acta Crystallogr., 16* (1963) 1139.

[57] G.M. Sheldrick, SHELXS-86, University of Göttingen, Göttingen, 1986; G.M. Sheldrick, in G.M. Sheldrick, C. Krüger and R. Goddard (eds.), *Crystallographic Computing 3*, Oxford University Press, Oxford, 1985, p. 175.

[58] B.A. Frenz, *Structure Determination Package VAX SDP*, Enraf-Nonius, Delft, Netherlands, 1987.

[59] J. Kopf and H.-Chr. Rübcke, *Program* CADSHEL, *Version 3.1*, University of Hamburg, Hamburg, 1993.

[60] SHELXTL-PLUS *Release 4.1*, Siemens Analytical X-ray Instruments, Madison, WI, 1990.

[61] G.M. Sheldrick, SHELXL-93, University of Göttingen, Göttingen, 1993.